Nucleon-nucleon effective potential in dense matter including rho-meson exchange.

L. Mornas[a], E. Gallego[b] and A. Pérez[b]

(a) *Departamento de Física, Universidad de Oviedo, E-33007 Oviedo (Asturias) Spain*

(b) *Departamento de Física Teórica Universidad de Valencia, E-46100 Burjassot (Valencia) Spain.*

July 25, 2013

Abstract

We obtain the RPA summed one-meson exchange potential between nucleons in symmetric nuclear matter at zero temperature, from a model which includes ρ, σ, ω and π mesons. The behavior of rho mesons inside the medium is first discussed using different schemes to extract a finite contribution from the vacuum polarization. These schemes give qualitatively different results for the in-medium rho mass. The results are discussed in connection with the non-renormalizability of the model. We next study the modified potential as density increases. In the intermediate distance range, it is qualitatively modified by matter and vacuum effects. In the long-distance range ($r > 2$ fm), one observes the presence of oscillations, which are not present in free-space. Features on this distance range are insensitive to the renormalization scheme.

1 Introduction

Quantum Hadrodynamics (QHD) designates a class of models in which nuclear interactions are described through *effective* relativistic Lagrangians of nucleons coupled to different kinds of mesons. Such models have been successfully used during the past decades to study very different situations, such as nucleon-nucleon scattering processes in free space [1] or the nuclear many-body problem [2] (for a recent review of QHD models, see [3]). In vacuum, the one-boson exchange approximation gives a reasonable approximation to nucleon-nucleon scattering data.

The situation becomes more complicated in dense nuclear matter since higher-order diagrams have to be taken into account. It is known for example that short range correlations arise due to the hard repulsive core in the free potential. An important achievement of the late eighties was the reproduction of saturation properties by parameter-free, (relativistic) Dirac-Brueckner G-matrix calculations [4, 5]. In this approach, repeated exchange of free mesons give rise to an effective potential with a smoothened repulsive core. On the other hand, it is also well-known that effects coming from the Random Phase Approximation (RPA) will modify the two-particle interaction at high densities.

For example, in QED the lowest-order interaction potential between two static charges is the usual Coulomb potential. Inside a plasma, RPA effects modify the photon propagator, and correspondingly one obtains a screened Debye potential. At larger distances, new phenomena appear. If the temperature is sufficiently low, the potential becomes oscillatory and damped as some power-law of the distance. These are the so-called *Friedel oscillations* [6], and are originated by the sharp profile of the Fermi surface at low temperatures. Friedel oscillations are supported by a large body of experimental evidence in metallic alloys (see *e.g.* [7]).

Similar screening effects are encountered in a QCD quark-gluon plasma when the quark-antiquark potential is calculated within the same approximations [8]. Such effects appear also if one considers the spatial dependence of static meson correlation functions at finite baryon density in the Nambu – Jona – Lasinio model [9]. In a nuclear plasma, the presence of the medium will also give rise to a modified interaction. The modifications of the potential due to RPA have been investigated so far in the case of the one-pion exchange [10] and for the Walecka σ - ω model [11, 12]. In both cases, a screened potential was obtained that differs from the one in vacuum . At long distances ($r \geq 2$ fm), the potential shows also an oscillatory behavior, as in the QED and QCD cases.

Our claim is that RPA may give important effects, both quantitative and qualitative, and has to be considered in many-body calculations of nuclear matter. As a matter of fact, it was shown [13] that RPA corrections give rise to a modification of the in-medium cross section of the same order of magnitude as Brueckner ones, and compatible with experimental data available so far. Other examples are the reduction of neutrino opacities in neutron star matter from RPA corrections of the NN interaction [14, 15] and the measurement of the electromagnetic response function in quasielastic electron scattering experiments [16].

Of course, both kinds of effects should eventually be considered. Within a diagrammatic perturbation expansion, they appear as summations of two distinct subsets of diagrams, namely particle-hole loops for the RPA, and ladder summation for the G-matrix mentioned above. Both are essential ingredients, since RPA summation is needed in order to describe long-range correlations, and, on the other hand, ladder summations are needed to create short-range correlations.

It would be desirable to develop some approach to incorporate both kind of summations in a systematic way. As discussed in [17], however, this can not be done simply by using the RPA modified potential as a driving term for ladder summation. Such an approach would lead to inconsistencies and double counting, and one has to look for more elaborated techniques. Parquet resummation [17] is the minimal extension that can accomplish this purpose, but its extension to relativistic strongly interacting systems still encounters technical difficulties. Besides theoretical problems, parquet techniques applied to interactions with a simpler structure, (scalar $\lambda\phi^4$ or QED) already lead to very complex results exceeding standard computational resources and tricky convergence issues. [1]

Before embarking on such an attempt, our aim will be more modest. We think that it is useful to check whether the RPA effects give rise to sizeable corrections in the density and momentum transfer ranges of interest. Actually, we already know from other contexts that the answer is positive [13, 15, 21]. Here we focus on the analysis of the modifications of the one-meson exchange potential due to RPA corrections to the meson propagator inside nuclear matter. We will pay special attention to the comparison of the modified potential, in contrast to the free-space potential. Keeping in mind the above considerations, since the RPA summation is not the only effect on the many-body problem, it cannot be used in naive ladder calculations. We insist, however, that this summation is a necessary (and important) piece of the problem, and deserves further study. In the course of the calculations, we obtain the modified meson propagator inside the medium, a result which is interesting by itself, since it allows us to study the effect of the medium on the meson propagation, the modification of the meson mass, the appearance of new branches, *etc.*

In this paper, we concentrate on these modifications within a model which includes ρ mesons, in addition to the π, σ and ω mesons already considered in the previous references. The inclusion of ρ mesons is a necessary ingredient in determining the proper isospin dependence of the nucleon-nucleon potential within meson exchange models [1]. Also, obtaining the rho propagator in dense matter will allow us to investigate how its in-medium mass changes as density increases. This issue has become important in the context of dilepton excess at low invariant masses observed in heavy ion collisions [22]. As we will show, however, the evolution of the ρ meson mass with density in this QHD model is very sensitive to the way in which the vacuum terms of the polarization are treated. This is due to the non-renormalizability of the derivative part of the ρ meson coupling which was introduced for phenomenological reasons. While renormalizability might not be a requirement in the case of *effective* models, one has to provide a prescription to eliminate the divergences that arise in these relativistic models *consistently*. As a matter of fact, one finds that, in renormalizable QHD models, vacuum effects eliminate the pathologies which appear when all vacuum terms are simply left out [23]. We will examine here several different prescriptions, leading to different consequences for the rho mass in nuclear matter.

This paper is organized as follows. In section 2 we define the model and calculate the corresponding RPA meson propagators in the medium. In section 3 we discuss how to extract a finite vacuum term from the vacuum polarization in the case of rho mesons. We give in section 4 general expressions for the one-boson exchange potential obtained from the modified propagator. In section 5 we discuss the rho-meson dispersion relations and effective mass in connection with the renormalization procedures discussed in section 3. Results concerning the in-medium potential are showed in section 6. We first consider only the exchange of rho mesons. After this, we give some plots which are obtained by adding all kind of mesons present in our model. Mechanisms which could be responsible for smearing away the Friedel oscillations present in this potential are discussed in Section 7. Finally, our main results are summarized and commented in Section 8. We have gathered in Appendix A and B the explicit formulae concerning the matter and vacuum part of the polarization tensor of rho mesons respectively. Appendix C contains the configuration space contributions from different mesons to

---

[1]Interesting attempts in this direction may also be found in a non relativistic formalism in [18, 19, 20].

2

the nucleon-nucleon potential.

2 Meson propagators in symmetric nuclear matter.

In this section, we describe the main steps necessary to obtain the meson propagators in the RPA approximation. The starting point will be a QHD model. For this, we adopt the one described by the following Lagrangian :

$$\mathcal{L} = \mathcal{L}_N + \mathcal{L}_\sigma + \mathcal{L}_\omega + \mathcal{L}_\pi + \mathcal{L}_\rho + \mathcal{L}_I + \mathcal{L}_{CC} \tag{1}$$

which assumes nucleons interacting with several kinds of mesons : σ, π, ρ and ω. In the latter equation, $\mathcal{L}_N$ corresponds to the nucleon Dirac free Lagrangian:

$$\mathcal{L}_N = (i/2)\,[\,\overline{\psi}\gamma\cdot\partial\,\psi - (\partial\,\overline{\psi})\cdot\gamma\,\psi\,] - m\,\overline{\psi}\,\psi \tag{2}$$

where $\psi = \begin{pmatrix} \psi_p \\ \psi_n \end{pmatrix}$ is the nucleon isospin-doublet (protons and neutrons) field with mass m,

$$\mathcal{L}_\sigma = (1/2)\,[\,(\partial^\nu\,\sigma)(\partial_\nu\,\sigma) - \mu_\sigma^2\,\sigma^2\,] \tag{3}$$

$$\mathcal{L}_\pi = (1/2)\,[\,(\partial^\nu\,\vec{\pi})(\partial_\nu\,\vec{\pi}) - \mu_\pi^2\,\vec{\pi}^2\,] \tag{4}$$

$$\mathcal{L}_\rho = -(1/2)\,[\,(1/2)\,\vec{R}_\rho^{\,\mu\nu}\cdot\vec{R}_{\rho\mu\nu} - \mu_\rho^2\,\vec{\rho}^{\,\nu}\cdot\vec{\rho}_\nu\,] \tag{5}$$

$$\mathcal{L}_\omega = -(1/2)\,[\,(1/2)\,F_\omega^{\mu\nu}\cdot F_{\omega\mu\nu} - \mu_\omega^2\,\omega^\nu\cdot\omega_\nu\,] \tag{6}$$

are the free Lagrangians for the mesons, with masses μ_i (i=σ, π, ρ and ω). $\mathcal{L}_I$ gives the meson-nucleon interaction. We have adopted simple Yukawa couplings for the σ, π and ω mesons. For the ρ-meson we added a tensor term [1]. Therefore, we have :

$$\mathcal{L}_I = \quad g_\sigma\,\overline{\psi}\,\sigma\,\psi + g_\omega\,\overline{\psi}\gamma^\mu\,\omega_\mu\,\psi - i\,g_\pi\,\overline{\psi}\,\gamma^5\,\vec{\tau}\cdot\vec{\pi}\,\psi$$
$$+ g_\rho\,\overline{\psi}\,\gamma^\mu\,\vec{\tau}\cdot\vec{\rho}_\mu\,\psi - \frac{f_\rho}{2m}\,\overline{\psi}\,\sigma^{\mu\nu}\,\psi\,\vec{\tau}\cdot\partial_\nu\,\vec{\rho}_\mu \tag{7}$$

with the following notations :

$$F_\omega^{\mu\nu} = \partial^\mu\,\omega^\nu - \partial^\nu\,\omega^\mu \tag{8}$$

$$\vec{R}_\rho^{\,\mu\nu} = \partial^\mu\,\vec{\rho}^{\,\nu} - \partial^\nu\,\vec{\rho}^{\,\mu} \tag{9}$$

Finally, $\mathcal{L}_{CC}$ contains the counterterms necessary to eliminate the divergences from the vacuum polarization. We will discuss this topic in more detail in the next section .

From Eq. (1) one can derive the equations of motion for the nucleons and mesons. In order to obtain the meson propagators, we have used the linear response theory around a given ground state of the meson-nucleon plasma. Our formalism is based on the introduction of Wigner functions. This formalism has been described in several papers in connection with the nucleon-nucleon interaction in a nuclear medium [11, 23, 24]. We will give here only the main steps relevant to the model adopted above, and refer the reader to these papers (and references therein) for a detailed description of the method.

The Wigner function for the nucleons is defined by :

$$F(x,p) = <\hat{F}(x,p)> = tr\left[\hat{\rho}_E\,\hat{F}(x,p)\right] \tag{10}$$

where $\hat{F}(x,p)$ represents the nucleon Wigner operator

$$\hat{F}(x,p) = \frac{1}{(2\pi)^4}\int d^4R\,e^{-ipR}\,\overline{\psi}\,(x+\frac{R}{2})\otimes\psi\,(x-\frac{R}{2}) \tag{11}$$

and $\hat{\rho}_E$ is the equilibrium density matrix operator. For a system at a given temperature T allowing for particle number variation, this is given by the Grand Canonical operator. Given a quantum operator $\hat{O}$, the statistical average is defined, as in Eq. (10), by

$$<\hat{O}> = tr\left[\hat{\rho}_E\,\hat{O}\right] \tag{12}$$

(the symbol tr means the trace with respect to the quantum states available to the system).

We assume that equilibrium can be described by the Hartree approximation. Within this approximation, meson fields are treated as classical fields and replaced by their statistical averages. These are furthermore restricted by symmetry properties. For symmetric nuclear matter, only $< \sigma >$ and the time-like component $< \omega^0 >$ survive [2] (all other meson mean fields are zero). This means that the nuclear background is described by the Walecka model. The mean-field values have to be obtained self-consistently, by solving the implicit equations

$$\mu_\sigma^2 \ < \sigma > = \ g_\sigma Tr \int d^4p \ F_H(p) \tag{13}$$

$$\mu_\omega^2 \ < \ \omega^0 > = \ - g_\omega \ Tr \int d^4p \ \gamma^0 F_H(p) \tag{14}$$

Here, Tr stands for the spin-isospin trace. In a spin saturated system, parity conservation implies $< \pi >= 0$. The value of the ρ mean field is related to the difference between neutron and proton densities, and since we are working in symmetric nuclear matter, we have $< \rho >= 0$.

The nucleon Wigner function in the Hartree approximation is given by

$$F_H(p) \ = \ (\gamma \cdot P + M) \ \begin{pmatrix} f(p) & 0 \\ 0 & f(p) \end{pmatrix} \tag{15}$$

The nucleon effective mass is $M = m - g_\sigma < \sigma >$, and P^μ is defined by $P^\mu = p^\mu + g_\omega < \omega^\mu >$. The last matrix in Eq. (15) corresponds to the isospin structure of $F_H(p)$, and $f(p)$ is the relativistic distribution function of nucleons, defined by

$$f(p) \ = \ \frac{1}{(2\pi)^3} \ \delta(P^2 - M^2) \ [\Omega^+(p_0) + \Omega^-(p_0) - H(-P_0)] \tag{16}$$

where $H(x)$ is the Heaviside step function and $\Omega^+(p_0)$ $(\Omega^-(p_0))$ are the nucleon (anti-nucleon) occupation numbers:

$$\Omega^\pm(p_0) \ = \ H(\pm P_0) \ \frac{1}{[\ 1 + e^{\beta(p_0 \mp \mu)}\ ]} \tag{17}$$

In the latter equation, μ is the nucleon chemical potential and $\beta = 1/T$ (we take the Boltzmann constant $k_B = 1$).

The next step in the linear response formalism is made by introducing small perturbations of the meson fields and the nucleon Wigner function around their Hartree values. Therefore, one has to replace :

$$\begin{aligned}
\sigma(x) & \rightarrow & < \sigma > + \delta \sigma(x) \\
\omega^\mu(x) & \rightarrow & < \omega^\mu > + \delta \omega^\mu(x) \\
\vec{\pi}(x) & \rightarrow & \delta \vec{\pi}(x) \\
\vec{\rho}^\mu(x) & \rightarrow & \delta \vec{\rho}^\mu(x) \\
F(x,p) & \rightarrow & F_H(p) + \delta F(x,p)
\end{aligned} \tag{18}$$

in the corresponding equations of motion, and consider only terms which are linear in the perturbations (notice that $< \vec{\pi} >=< \vec{\rho}^\mu >= 0$, as discussed above). One then obtains a system of coupled equations which can be solved for $\delta F(x,p)$. When substituted in the remaining equations, it gives a system of equations for the meson sector. For symmetric nuclear matter, the resulting system is considerably simplified. First, the pions and the rho mesons decouple from the rest. Only the σ and ω mesons are mixed together. However, the corresponding $\sigma + \omega$ equations are the same that appear in the Walecka model [11, 25]. Similarly, one reproduces for pions the well-known results [2, 23]. For this reason, we will concentrate here on the rho mesons. In this case, because of isospin symmetry, the equations of motion are the same for ρ^+, ρ^- and ρ^0, and can be written as :

$$D^{\mu\nu}(k) \ \delta\rho_\nu \equiv \ [-k^\mu k^\nu + (\ k^2 - \mu_\rho^2\ ) g^{\mu\nu} + \Pi_\rho^{\mu\nu}(k)\ ] \ \delta\rho_\nu \ = \ 0 \tag{19}$$

Here, $\Pi_\rho^{\mu\nu}(k)$ is the ρ-meson polarization tensor due to NN particle-hole loops. Explicitly,

$$\Pi_\rho^{\mu\nu} \ = \ \int d^4p \ Tr \left[(\gamma.(p - \frac{k}{2}) + M)(g_\rho\gamma^\mu + \frac{f_\rho}{2m}\sigma^{\mu\alpha}k_\alpha)(\gamma.(p + \frac{k}{2}) + M)(g_\rho\gamma^\nu - \frac{f_\rho}{2m}\sigma^{\nu\beta}k_\beta) \right] \ \times$$

$$\times \ \frac{f(p - k/2) - f(p + k/2)}{p.k} \tag{20}$$

4

(Analytical formulae are given in Appendices A and B). This tensor can be decomposed into two terms (we omit Lorentz indices):

$$\Pi_\rho(k) \;=\; \Pi_\rho^{mat}(k) \;+\; \Pi_\rho^{vac}(k) \tag{21}$$

The *matter* polarization, $\Pi_\rho^{mat}(k)$ vanishes in free space, i.e. at zero density and temperature. The second, *vacuum* term $\Pi_\rho^{vac}(k)$, gives a non-zero contribution even in free space. It contains divergent integrals from which one has to extract a finite contribution. This will be discussed in the next section.

The ρ-meson propagator in the medium $G(k)$ can be obtained by analyzing the response of the meson field against external nuclear sources. This procedure has been described in detail in [11]. As showed in this reference, the resulting propagator is given, in a matrix form, by

$$G(k) = - \left[D(k) \right]^{-1} \tag{22}$$

and obeys the Dyson equation (also written matricially). This equation, graphically represented in Fig. 1, reads

$$G(k) = G^0(k) + G^0(k)\Pi_\rho(k)G(k) \tag{23}$$

where $G^0(k)$ is the non-interacting ρ-meson propagator in vacuum. Eq. (19) can be analyzed with more detail by choosing a particular frame with the z-axis along the direction of $\vec{k}$, in such a way that $k^\mu = (w, 0, 0, q)$. Then, the only non-vanishing components of the polarization are $\Pi_\rho^{00}(k)$, $\Pi_\rho^{11}(k) = \Pi_\rho^{22}(k)$, $\Pi_\rho^{03}(k) = \Pi_\rho^{30}(k)$ and $\Pi_\rho^{33}(k)$. Eq. (19) then becomes

$$\begin{bmatrix} D^{00}(k) & 0 & 0 & D^{03}(k) \\ 0 & D^{11}(k) & 0 & 0 \\ 0 & 0 & D^{22}(k) & 0 \\ D^{30}(k) & 0 & 0 & D^{33}(k) \end{bmatrix} \times \begin{bmatrix} \delta\rho_0(k) \\ \delta\rho_1(k) \\ \delta\rho_2(k) \\ \delta\rho_3(k) \end{bmatrix} = 0 \tag{24}$$

where

$$D^{00}(k) \;=\; -\,(\, q^2 \;+\; \mu_\rho^2 \;-\; \Pi_\rho^{00}(k)\,) \tag{25}$$

$$D^{11}(k) = D^{22}(k) \;=\; -\,(\, k^2 \;-\; \mu_\rho^2 \;-\; \Pi_\rho^{11}(k)\,) \tag{26}$$

$$D^{33}(k) \;=\; -w^2 \;+\; \mu_\rho^2 \;+\; \Pi_\rho^{33}(k) \tag{27}$$

$$D^{03}(k) = D^{30}(k) \;=\; -wq \;+\; \Pi_\rho^{03}(k) \tag{28}$$

The dispersion relations can now be obtained by equating to zero the determinant of Eq. (24), which can be factored out into two terms :

$$|D(k)| \;=\; (D^{11}(k))^2 . \begin{vmatrix} D^{00}(k) & D^{03}(k) \\ D^{30}(k) & D^{33}(k) \end{vmatrix} \;=\; 0 \tag{29}$$

We obtain two equations, corresponding to *transverse* and *time-longitudinal* modes. These are given, respectively, by :

$$k^2 \;-\; \mu_\rho^2 \;-\; \Pi_\rho^{11}(k) \;=\; 0 \tag{30}$$

and

$$k^2 \;-\; \mu_\rho^2 \;-\; k^2/q^2 \, \Pi_\rho^{00}(k) \;=\; 0 \tag{31}$$

It is convenient to give these results in a fully covariant form. The ρ meson polarization can be decomposed as

$$\Pi_\rho^{\mu\nu} \;=\; -\Pi_{\rho T} T^{\mu\nu} - \Pi_{\rho L} L^{\mu\nu} \quad \text{with}$$

$$T^{\mu\nu} \;=\; g^{\mu\nu} - \frac{k^\mu k^\nu}{k^2} - \frac{\eta^\mu \eta^\nu}{\eta^2} \quad ; \quad L^{\mu\nu} = \frac{\eta^\mu \eta^\nu}{\eta^2} \quad ; \quad \eta^\mu = u^\mu - \frac{k.u}{k^2} k^\mu \tag{32}$$

where u^μ is the 4-velocity of the medium. $\Pi_{\rho T}$ and $\Pi_{\rho L}$ are Lorentz scalars representing the transverse and longitudinal components of the polarization. The dispersion relations read

$$k^2 - \mu_\rho^2 + \Pi_{\rho T} = 0 \quad ; \quad k^2 - \mu_\rho^2 + \Pi_{\rho L} = 0 \tag{33}$$

5

The propagator is obtained by inversion of the dispersion relation, and is given in the general case by

$$G_\rho^{\mu\nu} = -G_{\rho L} L^{\mu\nu} - G_{\rho T} T^{\mu\nu} + \frac{1}{\mu_\rho^2} \frac{k^\mu k^\nu}{k^2} \quad ; \qquad G_{\rho L} = \frac{1}{k^2 - \mu_\rho^2 + \Pi_{\rho L}} \quad ; \qquad G_{\rho T} = \frac{1}{k^2 - \mu_\rho^2 + \Pi_{\rho T}} \qquad (34)$$

In the referential where the fluid is at rest $u^\mu = (1, \vec{0})$, we have the following relations:

$$\Pi_{\rho L} = - k^2/q^2 \, \Pi_\rho^{00}(k) \qquad ; \qquad \Pi_{\rho T} = - \, \Pi_\rho^{11}(k) \qquad (35)$$

3 Vacuum polarization

In this section we discuss the procedure to extract a finite contribution from the vacuum polarization tensor. In the case of the σ and ω, or π mesons with a pseudoscalar coupling, the Lagrangian is renormalizable. This means that divergences can be eliminated consistently, at all orders, by introducing appropriate counterterms in the Lagrangian and imposing some physical conditions. This has been discussed in several papers; for a discussion within the formalism of Wigner functions see [23, 24, 26]. As pointed out in these references, the vacuum polarization gives an important contribution and eliminates some of the pathologies that appear in the *semi-classical approximation* (when all vacuum terms are simply discarded [2]). Therefore, one would like to conserve vacuum effects. Here, however, there is an important difference when considering the rho mesons. As a matter of fact, due to the derivative coupling appearing in Eq. (7), the Lagrangian becomes non-renormalizable, which implies that the counterterms needed to compensate the infinities at a given order of approximation will not be valid at higher orders. Nevertheless, it is still possible to eliminate the divergences *at a given order* by the procedure described below.

The method proceeds by dimensional regularization and the introduction of a counterterm Lagrangian.

The vacuum contribution arises from the last term $-H(-P_0)$ in Eq. (16). Since the only tensors at our disposal in vacuum are $g^{\mu\nu}$ and $k^\mu k^\nu$, and $\Pi_{\rho\ vac}^{\mu\nu}$ should be orthogonal to $k^\mu k^\nu$, it must be of the form:

$$\Pi_{\rho ren}^{\mu\nu}(k) \;=\; -Q^{\mu\nu} \, \frac{I(k)}{4\pi} \qquad (36)$$

where

$$Q^{\mu\nu}(k) \;=\; \frac{k^\mu k^\nu}{k^2} \;-\; g^{\mu\nu} \qquad (37)$$

After performing the trace, a straightforward calculation leads to

$$\Pi_{\rho\ vac}(k) \;=\; -\frac{16}{3} \frac{g_\rho^2}{(2\pi)^3} \mathcal{I}_1 - \frac{4}{3} \frac{g_\rho^2}{(2\pi)^3} (2M^2 k^2 + k^4)\mathcal{I}_2 - \frac{8}{3} \left(\frac{f_\rho}{2m}\right)^2 \frac{k^2}{(2\pi)^3} \mathcal{I}_1 - \frac{2}{3} \left(\frac{f_\rho}{2m}\right)^2 \frac{k^4}{(2\pi)^3}(8M^2 + k^2)\mathcal{I}_2$$

$$-\frac{8Mk^4}{(2\pi)^3} \left(\frac{f_\rho}{2m}\right) g_\rho \mathcal{I}_2 \qquad (38)$$

The integrals $\mathcal{I}_1$ and $\mathcal{I}_2$ diverge. These divergences can be extracted by the procedure of dimensional regularization

$$\mathcal{I}_1 \;=\; \int d^4p \, \delta(p^2 - M^2) \, H(-p_0) \quad ; \qquad \mathcal{I}_1^{reg} = \pi M^2 \left[-\frac{1}{\epsilon} + \ln\left(\frac{M}{m}\Lambda_1\right) \right] \qquad (39)$$

$$\mathcal{I}_2 \;=\; \int d^4p \, \frac{\delta(p^2 - M^2) \, H(-p_0)}{(p.k)^2 - k^4/4} \quad ; \qquad \mathcal{I}_2^{reg} = -\frac{2\pi}{k^2} \left[-\frac{1}{\epsilon} + \ln\left(\frac{M}{m}\Lambda_2\right) + \theta(k^2, M^2) \right] \qquad (40)$$

$\theta(k^2, M^2)$ is a known finite function given in Appendix B. Here, ϵ is an infinitesimal quantity and Λ_1, Λ_2 are arbitrary finite constants. Therefore, there appear the following divergences in $\Pi_{\rho\ vac}$ when $\epsilon \to \infty$:

$$\frac{1}{\epsilon} \quad \text{in the } g_\rho^2 \text{ term}, \qquad \frac{M}{\epsilon} \quad \text{in the } \frac{f_\rho}{2m} g_\rho \text{ term}, \qquad \frac{M^2}{\epsilon} \quad \text{and} \quad \frac{k^2}{\epsilon} \quad \text{in the } \left(\frac{f_\rho}{2m}\right)^2 \text{ term} \qquad (41)$$

---

[2]Moreover, the vacuum contribution depends on the plasma thermodynamical state, so that it can not be simply subtracted in a fully consistent way.

At the *one-loop level*, it is possible to compensate the divergences by adding the following counterterms to the Lagrangian:

$$\mathcal{L}^{\rho}_{CC} = \left\{ (A \; + \; B \, \sigma \; + \; C \, \sigma^2 \;) \; \vec{R}^{\mu\nu} \cdot \vec{R}_{\mu\nu} \; + \; D \; (\partial_\alpha \, \vec{R}_{\mu\nu}) \cdot (\partial^\alpha \, \vec{R}^{\mu\nu}) \right\} \tag{42}$$

in which A, B, C, D are constants to be determined by the renormalization procedure. In order to obtain the finite (renormalized) vacuum polarization, we have followed the same subtraction scheme as we used for the other mesons [23]. Namely, we first obtain the rho field equation from the generalized Euler equation[3]

$$\frac{\partial \mathcal{L}}{\partial \rho_\nu} - \partial_\mu \left(\frac{\partial \mathcal{L}}{\partial (\partial_\mu \rho_\nu)} \right) + \partial_\alpha \partial_\mu \left(\frac{\partial \mathcal{L}}{\partial (\partial_\alpha \partial_\mu \rho_\nu)} \right) = 0 \tag{43}$$

with the full Lagrangian including the counterterms. After linearizing and Fourier transforming, the dispersion equation (19) reads

$$\left[-k^\mu k^\nu + (k^2 - \mu_\rho^2) g^{\mu\nu} + \Pi_\rho^{\mu\nu} + (A + B\sigma + C\sigma^2 + Dk^2)(k^\mu k^\nu - k^2 g^{\mu\nu}) \right] \delta\rho_\nu = 0 \tag{44}$$

Now the vacuum rho polarization can be made finite if A, B, C, D consist of an infinite part cancelling the divergences we have pointed out in Eq. (41), and a finite part which we now proceed to determine on the basis of physical arguments. We will have

$$
\begin{aligned}
\Pi^{\mu\nu}_{\rho\,ren} &= \Pi^{\mu\nu}_{\rho\,vac} + (A + B\sigma + C\sigma^2 + Dk^2)(k^\mu k^\nu - k^2 g^{\mu\nu}) \\
&= \left\{ \frac{g_\rho}{3\pi^2} \left[\ln \frac{M}{m} + \theta + \frac{2M^2}{k^2}(\theta - 1) \right] + \left(\frac{f_\rho}{2m} \right)^2 \frac{1}{6\pi^2} \left[6M^2 \ln \frac{M}{m} + 8M^2\theta + k^2 (\ln \frac{M}{m} + \theta) \right] \right. \\
&\quad \left. + \frac{2M}{\pi^2} \left(\frac{f_\rho}{2m} \right) g_\rho \left[\ln \frac{M}{m} + \theta \right] - (\alpha + \beta \, \sigma + \gamma \, \sigma^2 + \delta k^2) \right\} \left\{ k^2 g^{\mu\nu} - k^\mu k^\nu \right\}
\end{aligned} \tag{45}
$$

with the decomposition

$$
\begin{aligned}
A &= \alpha + \frac{g_\rho^2}{3\pi^2} \left[-\frac{1}{\epsilon} + \ln \Lambda_2 - \frac{1}{2} \right] + \frac{2m}{\pi^2} \left(\frac{g_\rho f_\rho}{2m} \right) \left[-\frac{1}{\epsilon} + \ln \Lambda_2 - \frac{1}{2} \right] + \left(\frac{f_\rho}{2m} \right)^2 \frac{m^2}{3\pi^2} \left[-\frac{3}{\epsilon} + 4 \ln \Lambda_2 - \ln \Lambda_1 - 2 \right] \\
B &= \beta - \frac{2g_\sigma}{\pi^2} \left(\frac{g_\rho f_\rho}{2m} \right) \left[-\frac{1}{\epsilon} + \ln \Lambda_2 - \frac{1}{2} \right] - \left(\frac{f_\rho}{2m} \right)^2 \frac{2mg_\sigma}{3\pi^2} \left[-\frac{3}{\epsilon} + 4 \ln \Lambda_2 - \ln \Lambda_1 - 2 \right] \\
C &= \gamma + \left(\frac{f_\rho}{2m} \right)^2 \frac{g_\sigma^2}{3\pi^2} \left[-\frac{3}{\epsilon} + 4 \ln \Lambda_2 - \ln \Lambda_1 - 2 \right] \\
D &= \delta + \left(\frac{f_\rho}{2m} \right)^2 \frac{1}{6\pi^2} \left[-\frac{1}{\epsilon} + \ln \Lambda_2 - \frac{1}{2} \right]
\end{aligned} \tag{46}
$$

In order to determine the finite constants $\alpha, \beta, \gamma, \delta$, some physical constraints have to be imposed. The standard [25] requirements are that:

* (1) The vacuum polarization has to vanish in free space, when the rho meson is on its mass shell (here, "shell"$=\{k^2 = \mu_\rho^2, M = m, \sigma = 0\}$):

$$\Pi_{\rho \; vac|\text{shell}} = 0, \tag{47}$$

* (2) The field equation can be written in the standard form by defining effective coupling constants g_{eff} and f_{eff}. Requiring that the effective coupling be equal to the bare one in vacuum leads to the condition

$$\frac{\partial \Pi_{\rho \; vac}}{\partial k^2}\bigg|_{\text{shell}} = 0 \tag{48}$$

* (3) The new couplings $\sigma R_{\mu\nu} R^{\mu\nu}$, $\sigma^2 R_{\mu\nu} R^{\mu\nu}$, that we had to introduce in order to subtract the infinities, should not appear in the dispersion relation on the rho meson mass shell, leading to the conditions

$$\frac{\partial \Pi_{\rho \; vac}}{\partial \sigma}\bigg|_{\text{shell}} = 0 \tag{49}$$

---

[3]The D counterterm makes this generalization necessary

and
* (4)

$$\frac{\partial \Pi_{\rho \ vac}}{\partial \sigma^2}\bigg|_{\text{shell}} = 0 \tag{50}$$

This amounts to four relations to determine the four constants $\alpha, \beta, \gamma, \delta$.

Alternative sets of conditions can be imposed, leading to different expressions of the vacuum polarization. In particular, we can recover the renormalization scheme suggested by Shiomi and Hatsuda [27] as a special case of our general formalism. We have also tried these alternative schemes in our calculations in order to investigate the influence of the treatment of the vacuum. As we will see in section (5.3), the various schemes predict a completely different behavior of the in-medium rho meson mass as density increases.

The peculiarities of each scheme, outline of derivation and corresponding analytical expressions are given in Appendix B. They can be subdivided into two classes: The first class of schemes comprises those which are designed not to introduce new couplings with the σ mesons (conditions (3) and (4) of the method outlined above). This is the case of the scheme presented here, labelled "scheme 1" and of a very similar one labelled "scheme 2". With a different point of renormalization, the scheme presented in the case of the σ meson in the classical paper of Kurasawa and Suzuki [28] also belongs to this class. We applied it to the ρ meson and labelled the result "scheme 6". The second class of renormalization schemes preserves the structure of the regularized expression, introducing counterterms $\alpha + \beta\sigma + \gamma\sigma^2$ so that they can be factorized into $\alpha M^2/m^2 = \alpha(m - g_\sigma\sigma)^2/m^2$. As a result, conditions (3) and (4) cannot be fulfilled anymore. We called the scheme obtained in this way "scheme 3". The method of Shiomi and Hatsuda (scheme 5) and a related one used by Sarkar *et al.* [29] ("scheme 4") belong to this class.

The advantages and caveats of the respective renormalization schemes will be further discussed in a forthcoming work[30].

4 One-boson exchange potential in the medium.

In this section we calculate the one-boson exchange potential obtained after RPA summation. As mentioned in the previous section, when the background is symmetric nuclear matter, rho mesons (and pions as well) decouple from the other mesons, whereas σ and ω mesons are coupled together. Therefore, the total potential shows the following structure :

$$V = V^{\sigma+\omega} + V^\pi + V^\pi \tag{51}$$

where $V^{\sigma+\omega}, V^\pi$ and V^π are obtained by $\sigma + \omega$, one-pion and one-rho exchange, respectively. Our method follows a similar procedure to the construction of the one-boson exchange potential in vacuum [1]. The essential difference is that free meson propagators are replaced by in-medium propagators. Also, the external nucleon lines correspond to in-medium spinors, as they arise by solving the nucleon Dirac equation in the Hartree approximation. It is important to mention, however, that one arrives to the above result by computing the energy associated to a pair of interacting nucleons inside the plasma, a result which ensures that no double counting has been made. The method has been given in detail in [11], and applied to the calculation of $V_{\sigma+\omega}$.

As in the free case, we expand the resulting potential in powers of $\frac{p}{M}$, where p represents the momenta of the external nucleons, and keep only terms of the order $\sim \left(\frac{p}{M}\right)^2$. This has the advantage to simplify the spin structure of the nucleon-nucleon potential. For degenerate nuclear matter, one has $p \sim p_F$, where p_F is the nucleon Fermi momentum. If the density is close to saturation, the next term in the expansion would be a small correction of the order $\left(\frac{p}{M}\right)^4 \sim \left(\frac{0.3}{0.7}\right)^4$. Of course, if density is much larger, higher order terms in the above expansion should be taken into account.

In constructing the one-rho potential one has to take into account the diagram shown in Fig. 2, where the double line represents the in-medium rho-meson propagator, given by Eqs. (22 − 28) and Eq. (34). The amplitude corresponding to this diagram is given by

$$\begin{aligned}
\mathcal{M}_\rho &= -\left\{ \left[\chi_{1'}^\dagger \, \overline{u}(\vec{p'}_1, s'_1) \right] \left(i \, g_\rho \, \gamma^\mu - \frac{f_\rho}{2m} \, \sigma^{\mu\beta}(p_1{}' - p_1)_\beta \right) \, \tau_1^a \, \left[u(\vec{p}_1, s_1) \, \chi_1 \, \right] \right\} \\
&\quad \delta_{ab} \, G_{\mu\nu}(k) \, \left\{ \left[\chi_{2'}^\dagger \, \overline{u}(\vec{p'}_2, s'_2) \right] \left(i \, g_\rho \, \gamma^\nu - \frac{f_\rho}{2m} \, \sigma^{\nu\alpha}(p_2{}' - p_2)_\alpha \right) \, \tau_2^b \, \left[u(\vec{p}_2, s_2) \, \chi_2 \, \right] \right\}
\end{aligned} \tag{52}$$

In this equation, χ_1, χ_2 stand for the quantum states of the initial nucleons with four-momenta p_1 and p_2. They have associated spinors $u(\vec{p}_1, s_1)$ and $u(\vec{p}_2, s_2)$. Similarly, the prime indicates the corresponding magnitudes for final nucleons. The isospin operators τ_1^a, τ_1^b $(a, b = +, -, 0)$ label the associated rho charged fields. From Eq. (52) we obtain the one-rho exchange potential, by using the procedure outlined above. In the center-of-mass frame (CM) of the nucleons[4], the potential is given by:

$$
\begin{aligned}
V_\rho(\vec{q}, \vec{Q}) &= \left\{ g_\rho^2 \left[-G_{\rho L} \left(1 + \frac{\vec{Q}^2}{2M^2} - \frac{\vec{q}^2}{8M^2} + \frac{i}{2M^2}(\vec{q} \wedge \vec{Q}).\vec{S} \right) \right. \right. \\
&\qquad \left. + G_{\rho T} \left(-\frac{\vec{Q}^2}{M^2} - \frac{i}{M^2}(\vec{q} \wedge \vec{Q}).\vec{S} + (\vec{\sigma}_1.\vec{\sigma}_2)\frac{\vec{q}^2}{4M^2} - \frac{(\vec{\sigma}_1.\vec{q})(\vec{\sigma}_2.\vec{q})}{4M^2} \right) \right] \\
&\quad + 4M\, g_\rho \left(\frac{f_\rho}{2m} \right) \left[-G_{\rho L} \left(-\frac{\vec{q}^2}{4M^2} + \frac{i}{2M^2}(\vec{q} \wedge \vec{Q}).\vec{S} \right) \right. \\
&\qquad \left. + G_{\rho T} \left(-\frac{i}{2M^2}(\vec{q} \wedge \vec{Q}).\vec{S} + (\vec{\sigma}_1.\vec{\sigma}_2)\frac{\vec{q}^2}{4M^2} - \frac{(\vec{\sigma}_1.\vec{q})(\vec{\sigma}_2.\vec{q})}{4M^2} \right) \right] \\
&\quad \left. + 4M^2 \left(\frac{f_\rho}{2m} \right)^2 \left[G_{\rho T} \left((\vec{\sigma}_1.\vec{\sigma}_2)\frac{\vec{q}^2}{4M^2} - \frac{(\vec{\sigma}_1.\vec{q})(\vec{\sigma}_2.\vec{q})}{4M^2} \right) \right] \right\} \; \vec{\tau}_1 \cdot \vec{\tau}_2
\end{aligned}
\tag{53}
$$

In the latter equation, $\vec{\sigma}_i$ $(\vec{\tau}_i)$ represent the spin (isospin) Pauli matrices for the two $(i = 1, 2)$ interacting nucleons. In the chosen frame, initial nucleons have momenta $\vec{p}$ and $-\vec{p}$, whereas final nucleons are assumed to have momenta $\vec{p}\,'$ and $-\vec{p}\,'$. We have introduced the notations:

$$
\vec{q} = \vec{p} - \vec{p}\,' \quad ; \qquad \vec{Q} = (\vec{p} + \vec{p}\,')/2 \quad ;
$$

$$
G_{\rho L}(0, \vec{q}) = \frac{-1}{q^2 + \mu_\rho^2 - \Pi_\rho^{00}(0, \vec{q})} \quad ; \qquad G_{\rho T}(0, \vec{q}) = \frac{-1}{q^2 + \mu_\rho^2 + \Pi_\rho^{11}(0, \vec{q})}
\tag{54}
$$

Next we will construct the in-medium (RPA summed) nuclear potential in configuration space. This is done by Fourier transformation of the corresponding momentum-space magnitudes. Before proceeding, we include a phenomenological form factor in the nucleon-meson vertices. This amounts to making the replacements:

$$
\begin{aligned}
g_\alpha &\rightarrow g_\alpha \cdot \mathcal{F}_\alpha(q) \\
f_\rho &\rightarrow f_\rho \cdot \mathcal{F}_\rho(q) \\
\mathcal{F}_\alpha(q) &= \frac{\Lambda_\alpha^2 - \mu_\alpha^2}{\Lambda_\alpha^2 + q^2}
\end{aligned}
\tag{55}
$$

$(\alpha = \sigma, \omega, \pi, \rho)$ in all previous equations in momentum space. After some algebra, the configuration space potential can be decomposed in the following way [1]:

$$
\begin{aligned}
V(\vec{r}) &= V_c(r) - \frac{1}{2} \left(\nabla^2 V_{NL}(\vec{r}) + V_{NL}(\vec{r})\nabla^2 \right) \\
&\quad + V_{LS}(r)\, \vec{L} \cdot \vec{S} + V_{SS}(r)\, \vec{\sigma}_1 \cdot \vec{\sigma}_2 + V_T(r)\, S_{12}
\end{aligned}
\tag{56}
$$

with the following notations: $\vec{L}$ is the angular momentum operator, $\vec{S} = \frac{1}{2}(\vec{\sigma}_1 + \vec{\sigma}_2)$ is the total spin of the nucleons and S_{12} the tensor operator. In this way, $V_c(r)$ is the central part of the potential, $V_{LS}(r)$ is the spin-orbit, $V_{SS}(r)$ is the spin-spin, and $V_T(r)$ is the tensor potential. In addition to the spin structure, one has to include a factor $\vec{\tau}_1 \cdot \vec{\tau}_2$ in the pion and rho contributions (omitted here). The second term in Eq. (56) is non-local. Its contribution will depend on the explicit form of the two-nucleon wave function and, therefore, can not be directly plotted. For our analysis in the next section we will not consider this term.

Each one of the pieces in Eq. (56) has contributions from different meson exchanges ($\sigma + \omega$ sector, π or ρ). Their expressions can be found in Appendix C.

----

[4] We consider here the case where the rest frame of the background fluid coincides with the center of mass of the collision. For the effects due to a relative velocity between both frames, the reader is referred to [31]

5 Results for the rho-meson propagation

5.1 Choice of parameters

We will analyze the behavior of the in-medium potential as density changes, at zero temperature. Our calculations include the vacuum and matter polarization in the meson propagators. Since the vacuum contribution does not vanish at finite $\vec{q}$ in general, we cannot take directly the parameters available in the litterature. Instead, we must perform a fit anew for each one of renormalization schemes described in Appendix B. We have fitted the value of the coupling constants g_σ, g_ω, g_ρ, f_ρ and cutoff parameters Λ_σ, Λ_ω, Λ_π, Λ_ρ in such a way that, at zero density, the model reproduces as close as possible the Bonn 'Potential B' [1] (table A.3 in this reference). The value of the pion coupling g_π was kept constant since it is well known from experimental data. The values of meson masses are taken directly from this reference. However, we do not include the δ and η mesons in the fitting procedure. Since the Bonn potential has been adjusted to reproduce low-energy nucleon scattering data, we expect that our model can give a reasonable description to these experimental data. We have chosen to make this fit in the region from 0.5 to 2.5 fm for all mesons. The resulting parameters are given in Table 1, and the values of the obtained chi-squared for the different pieces of the potential appear in Table 2.

	g_σ	g_ω	g_ρ	f_ρ/g_ρ	Λ_σ	Λ_ω	Λ_π	Λ_ρ
Bonn B	10.6	17.55	3.36	6.1	1900	1850	1700	1850
set 1A	8.10	16.267	4.216	4.974	1630.55	1562.19	1179.48	1881.93
set 1B	7.55	15.817	3.390	5.115	1558.22	1550.12	729.40	1365.54
set 2A	7.83	15.783	3.718	4.996	1390.92	1493.97	976.30	1797.30
set 2B	7.59	16.091	3.882	4.319	1532.25	1521.51	690.48	1112.22
set 3A	8.54	15.910	3.862	5.811	1080.65	1441.00	1212.30	1638.73
set 3B	8.53	16.377	5.710	4.547	1329.54	1500.82	1150.89	1260.05
set 4A	7.22	14.624	3.303	7.033	1540.38	1629.70	1144.72	1375.11
set 6A	7.57	14.809	3.636	5.731	1626.54	1590.76	1125.17	1711.54

Table 1: Values the coupling constants and cutoffs which adjust the Bonn potential B [1] for each renormalization scheme

	$\chi^2(V_C)$	$\chi^2(V_{SS})$	$\chi^2(V_T)$	$\chi^2(V_{LS})$
set 1A	0.096	0.026	0.014	0.078
set 1B	0.136	0.232	0.019	0.179
set 2A	0.078	0.049	0.056	0.172
set 2B	0.123	0.182	0.061	0.203
set 3A	0.026	0.039	0.035	0.142
set 3B	0.038	0.065	0.031	0.082
set 4A	0.079	0.079	0.054	0.210
set 6A	0.087	0.034	0.069	0.191

Table 2: χ^2 values corresponding to the parameter sets given in Table 1, for each component of the NN potential: central (C), spin-spin (SS), tensor (T) and spin-orbit (LS)

In these tables, the number labelling each set is determined by the corresponding renormalization scheme (see Appendix B). The letter A means that the best fit for all components of the potential was looked for. As will be seen in the next section, the dispersion relation of the ρ meson may display heavy meson modes and, more annoyingly, zero-sound modes for too high values of the ρ meson cutoff. Therefore we performed the fit once again, but now with the constraint that a lower cutoff is used for the ρ meson in order to avoid the appearance of these spurious branches. The letter B corresponds such fits, and due to this restriction they come with slightly higher χ^2 values.

We do not give parameter sets for renormalization scheme 5, because this scheme was constructed by Shiomi and Hatsuda in such a way that the vacuum polarization vanishes identically (for all q) in the vacuum. In this case, the expression of Machleidt [1] is recovered exactly, therefore there is no need of readjusting the parameters and the original values of Machleidt (Bonn potential B) may be used.

5.2 Rho meson dispersion relations

With the above values of the meson parameters, we have first performed a numerical study of the rho-meson[5] dispersion relations defined by Eqs. (30), (31). Vacuum appears through the renormalization scheme discussed in Section 3. We use the renormalization scheme described in that section (scheme 1 of Appendix B), as well as alternative schemes described in Appendix B. A sample of the resulting branches are plotted in Figures 3 to 5 for longitudinal and transverse modes, for various values of the nucleon Fermi momentum $p_F = 0.3$, 0.4, 0.5 (all magnitudes are given in units of the nucleon bare mass m). In our model, this correspond to densities ρ_0, $2.37 \, \rho_0$ and $4.63 \, \rho_0$ with ρ_0 being the nuclear saturation density. The variables ω and q are defined by $k = (\omega, 0, 0, q)$, as in Section 2.

We at once observe that the dispersion relation strongly depends on the chosen renormalization scheme, both directly, and indirectly since it conditions the choice of parameters at the time of fitting the potential (see Table 1). Let us first discuss the general features of the transverse mode for parameter sets 1A to 6A, which were obtained by fitting the NN potential without imposing restrictions on the allowed range for each parameter.

In the timelike region, besides the normal branch, we also have two heavy meson branches in the general case. This kind of meson branches have been obtained in other models of QHD, and originate from vacuum effects [23, 24]. Such meson modes are present at densities corresponding to $p_F \geq 0.3$ for all renormalization schemes, with the exception of parameter set 4A, corresponding to the renormalization scheme of Sarkar [29]. It must be noted, however, that this parameter set has a value of the ρ meson cutoff appreciably lower than other A-sets. As will be discussed later, a smaller value of the cutoff has the effect of reducing or eliminating the heavy meson branches.

At high density, there appears moreover a zero sound branch in the spacelike region. This latter branch could have especially strong (and unpleasant) effects on our results for the potential, since it appears as a pole in the propagator. We found such a branch for renormalization schemes belonging to both classes considered in this work: in the "increasing rho mass" class, with parameter set 2A at $p_F > 0.4$ and also for the "decreasing rho mass" renormalization scheme of Shiomi and Hatsuda at $p_F > 0.6$. Nevertheless, we will see in the sequel that this pole can be eliminated by reducing the value of the ρ meson cutoff.

The longitudinal modes have a similar structure in the timelike region, with a normal branch and two heavy meson branches. In the spacelike region no zero sound branches were found.

In order to eliminate the spurious branches, it was possible to find a second series of parameter sets with stronger cutoffs for the ρ meson, at the cost of a slightly degraded quality of the fit. We called the resulting sets 1B, 2B and 3B. This permits to eliminate the zero sound branch at all densities investigated (up to $p_F = 2$) and to reduce or eliminate the heavy meson branches. It was moreover checked that the choice of a lower cutoff parameter does not affect appreciably the position of the normal branch.

The dispersion relations for parameter set 1B are shown in Figure 3. A moderate cutoff $\Lambda_\rho = 1365$ MeV was applied. The zero sound branch is now removed, but we still have heavy meson branches. The left panel displays the transverse modes. The right panel compares the transverse (thin line) to the longitudinal (thick line) modes for the normal branch. At $q = 0$ the transverse and longitudinal modes coincide; for finite q they differ only slightly. Finally, we note that the intercept of the normal branch with the $q = 0$ axis goes to higher frequencies with increasing p_F (or densities). This is related to the fact that the effective mass of the ρ meson increases with this renormalization schemes, as discussed in next section.

The dispersion relations for parameter set 2B are shown in Figure 4, now with a strong cutoff $\Lambda_\rho = 1112$ MeV. Only the normal branch remains for the transverse mode. The longitudinal modes are also appreciably cleaned, with only a persistent heavy meson mode at high momentum transfer. A still lower cutoff would eliminate it, but would spoil the accuracy of the fit of the NN potential.

In Figure 5 we show the transverse dispersion relation obtained with a renormalization scheme of the second ("decreasing rho mass") class. The parameter set used is 3B, with a reasonable ρ cutoff $\Lambda_\rho = 1260$ MeV, resulting in a clean dispersion relation: there only remains the normal branch. Moreover, the quality of the fit remains

---

[5]The analysis of the σ, ω and π dispersion relations has been performed in [23].

very good. We do not show the longitudinal modes since we found that longitudinal and transverse modes are indistinguishable. We note that the intercept of the normal branch with the $q = 0$ axis is lower at finite density than in vacuum, and slightly increases from p_F=0.3 to p_F=0.5, corresponding to the fact that the rho meson effective mass with this renormalization scheme first decreases with density and reaches a minimum around $p_F = 0.35$ (see next section).

We also programmed and plotted the dispersion relations obtained with schemes 4 to 6, but chose not to display them here . Scheme 6 ("Kurasawa-Suzuki") was found to be essentially similar to other schemes of the same class (1 and 2) but more problematic when we tried to remove the sound mode and heavy meson branches. For the dispersion relation obtained with the scheme 5 of Shiomi and Hatsuda [27] with the parameters of Machleidt Bonn potential B, we have again a normal branch and two heavy meson branches in the longitudinal as well as in the transverse modes. Moreover, a tiny zero sound branch also appears in the transverse mode at high enough densities ($\rho > 7 \, \rho_0$, $p_F < \sim 0.6$). We performed a fit with a lower value of Λ_ρ and found a parameter set which behaves essentially like case 3B. For the scheme of Sarkar *et al.* (scheme 4) we obtain only the normal branch for both transverse and longitudinal modes. This renormalization scheme is free from heavy meson branches and zero sound modes. This is due in part to the fact that the fit to the potential in vacuum requires in this case typically lower rho meson cutoffs of the order of 1300 MeV. Still we found this scheme more robust than the previous ones, since no such branches were found even for extreme values of parameters adjusting the potential.

5.3   Rho meson effective mass

From the dispersion relations one can obtain the in-medium mass μ_{eff}, defined as the solution $\mu_{eff} = \omega$ of the dispersion relations Eq. (30), (31) at $\vec{q} = 0$. The transverse and longitudinal modes yield the same effective mass, since the polarizations are equal in this limit. In Figs. 6-8 we show how μ_{eff} evolves, in units of the vacuum mass μ_ρ, as p_F grows (remember that $p_F/m = 0.3$ corresponds to saturation density). In particular, we wish to investigate the role of the vacuum on its behavior, in connection with the claim of Shiomi and Hatsuda [27] that the vacuum contribution solves this issue.

We first show in Figure 6 the effective mass obtained by keeping only the matter contribution in the rho meson polarization (thus neglecting the vacuum term). This figure was obtained with the parameter set of Machleidt potential B (see table 1). If we would limit ourselves to a moderate density and frequency, it would appear that the rho meson mass is slightly increasing. A closer inspection reveals, however, that the structure of the dispersion relation is more complex and has 3 solutions for $p_F < 0.246$ (that is, a density $\rho < 0.5\rho_0$), corresponding to anomalous branches intermingled with the normal one. At higher density, only the higher branch survives. This type of behavior is in fact well documented. It was first observed in the case of the ω meson by Lim and Horowitz [32] and also appears in the case of the pion [33]. Contrarily to a rather widespread belief, it is not cured by the introduction of a stronger form factor. As a matter of fact, we redraw on the same figure the rho mass for a low cutoff (1 GeV) and see that the problem, although less acute, is still present. Moreover, we cannot choose the cutoff as we please, since it was obtained from a fit of the nucleon-nucleon potential in the vacuum.

In the case of the σ, ω and π mesons, the situation is largely improved by introducing the vacuum term. There, a lower normal branch cleanly separates from higher heavy meson branches. Without any cutoff, two heavy meson branches appear at zero density and merge and disappear at high density. The heavy meson branches can thereafter be removed by the application of a reasonable cutoff. As we will see, the same occurs in the case of the rho meson.

In figure 7, the on-shell renormalization schemes 1 and 2 of Appendix B were used. The parameters were chosen so as to obtain the best fit of the nucleon-nucleon potential in each case (parameter sets 1A and 2A of table 1). We also plotted on the same figure the resulted obtained by adapting the scheme of Kurasawa and Suzuki for the σ, ω mesons to this case (parameter set 6A). In this figure and the next one, only the mass corresponding to the lower normal branch is represented. There also exist two branches at higher masses (typically 3.5 μ_ρ and 7 μ_ρ) which merge and disappear at very high density, which we do not show here. It is a common feature of all these renormalization schemes that the lower branch gives an in-medium mass which is larger than in vacuum. In all cases, the increase is quantitatively similar for all the three schemes, and somewhat stronger for scheme 6 of Kurasawa and Suzuki. On the other hand, the heavy meson branches largely depend on the value of the cutoff, so that this cutoff can be used to remove these branches altogether. As an example, we give in Table 1 a parameter set which makes it possible both to obtain a satisfactory fit of the potential and to remove the heavy meson branches (set 2B).

On the other hand, if one makes use of the renormalization scheme proposed by Shiomi and Hatsuda in [27], one then obtains a rho mass which decreases with density. We have re-derived the formulae given in this reference using our own methods (scheme 5 of Appendix B) and checked that our result is in agreement with theirs. The resulting effective mass is plotted in Figure 8. As advertised, the rho meson mass decreases until $p_F = 0.35$ (or $\rho = 1.6\rho_0$), and then slowly increases. We note that there also appear heavy meson branches. We plotted on the same figure the result obtained from a similar scheme used by Sarkar *et al.* [29] (scheme 4 of Appendix B). While Shiomi and Hatsuda subtract the vacuum at all momenta k, Sarkar *et al.* set the vacuum to zero at $k^2 = \mu_\rho^2$ in a way similar to our condition Eq. (47). The normal branch obtained from scheme 4 is quantitatively very similar to the result of Shiomi and Hatsuda.

These results are tantalizing since they are in agreement with the currently accepted concept of a decreasing rho meson mass based on other models and experimental data. Now, in order to interpret the contradiction which appears between schemes 1,2,6 on one hand, and 4,5 on the other hand, we have developped a further scheme (scheme 3). As further explained in Appendix B, the introduction of counterterms $(A + B\,\sigma + C\,\sigma^2)$ does not preserve in general the original structure of the diverging term proportional to $M^2 = (m - g_\sigma\sigma)^2$. It can be required that this M^2 structure be preserved by dropping conditions (49,50). The resulting effective mass is also plotted on Figure 8, and we see that it actually decreases as well.

The idea of a decreasing rho mass in the medium was popularized by the Brown and Rho scaling conjecture [34] as a result of chiral symmetry restoration. It allows to parametrize the in-medium mass of vector mesons as

$$\frac{\mu_{eff}}{\mu_\rho} \approx 1 - (0.18 \pm 0.05)\frac{\rho}{\rho_0} \tag{57}$$

as a function of the density ρ (written in units of the nuclear saturation density ρ_0). For example, as a consequence of QCD sum rules, Hatsuda and Lee [35] or Leinweber and Jin [36] obtain a decreasing mass. The use of QCD sum rules, however, was criticized for containing some uncertainties and inconsistencies with chiral perturbation theory [37]. Another caveat is the parametrization of the spectral function used in these calculations [38, 39], which further reduces the predictive power of QCD sum rules arguments. Finally, recent QCD sum rules calculations with an improved vacuum subtraction [40] further contributed mitigating the simple Brown-Rho decreasing mass picture.

Other calculations, based on chiral approaches (see *e.g.* [41], and [42] for a review) or quark-meson coupling models [43] also predict a slight lowering of the rho meson mass. In chiral models including a $\rho\pi\pi$ interaction piece (see also the brief discussion in this work, section 7.1), the rho mass is only slightly modified, the important effect there is the broadening of its spectral function. It is interesting to note that, depending on the renormalization scheme, the position of the maximum of the spectral function is shifted up- or downwards depending on the choice of the renormalization procedure ([44] *vs.* [45]). The theoretical situation is far to be settled, and there is a possibility for the rho mass to increase, rather to decrease, due to medium effects (see also *e.g.* [46, 47]).

There are a number of experiments in which it has been claimed that one can extract information about the vector mesons in a nuclear medium. In heavy-ion collisions experiments as HELIOS-3 [48] and CERES [49], the excess of dilepton production at invariant masses lower than the bare rho meson mass might be explained in the framework of the vector dominance model by assuming a dropping of the in medium rho-meson mass [22, 50, 51]. This interpretation is sometimes called, for short, the B/R (Brown-Rho) scenario. However, it has been pointed out that keeping a constant rho mass and introducing a medium modification of its width [52, 53] could also explain the dilepton excess. Friman and Pirner [54] have also argued that the contribution of higher resonances (*N(1720)) to the rho-meson self energy in matter plays an important role in shifting the strength to lower invariant masses. The 'broadening scenario' sometimes receives the name of R/W (Rapp-Wambach [53]) scenario.

For some time, measurements of polarization-transfer experiments with polarized protons seemed to favor the dropping-mass hypothesis as well [55, 56, 57]. New analyses of the results with a better treatment of relativistic effects, however, concluded that the data could be explained without this assumption [58].

In summary, the problem of how medium effects will modify the rho-meson properties is still not well settled, both from the theoretical and experimental points of view, although the possibility that its mass will be smaller at higher densities seems to be more favored. Future experiments, like HADES at GSI, will hopefully help clarifying this issue.

In our hadronic model, we have seen that the inclusion of the vacuum contribution largely affects the meson propagation in matter. Vacuum renormalization still allows for a increasing, as well as for a decreasing meson mass, and does not by itself settle the issue. If we believe that the rho meson mass should be decreasing, then a

renormalization scheme which preserves the original dependence in the nucleon effective mass should be chosen. But then, in order to be coherent, the same procedure has to be used for the σ, π and ω mesons as well [30] [6].

In view of this situation, we have made some comparisons using the two classes of renormalization schemes described above, each one of them giving a different behavior of the rho meson inside the nuclear medium.

6 Results for the RPA effective potential in the medium.

We shall now analyze the different components of the in-medium potential in position space, obtained in section 4, as density changes at $T = 0$. As discussed in that section, the mixing terms of the ρ-meson polarization with other mesons vanish if one considers symmetric nuclear matter, a circumstance which will allow us to consider first the contribution to the potential of this meson alone. Later, we shall add the contributions of the σ, ω and π mesons.

In performing the present analysis, it is useful to make the following division in the distance variable r, as was made in [11]:

a) In the *short-range* region $0 \leq r \leq 1$ fm, relativistic effects (beyond the quadratic approximation considered above) become essential. Also, in this distance range the extended structure of the nucleon must be properly taken into account. The introduction of form factors allows to simulate this effect for not-too-short distances, such as $0.5 \leq r \leq 0.8$ fm. For shorter distances, calculations from our model will not be reliable.

b) The *intermediate region* will be defined as the distance range $1 \leq r \leq 2$ fm. Within this range, the vacuum potential becomes quantitatively modified by medium and vacuum effects, as compared to the free-space potential.

c) In the *long-range* region : $r \geq 2$ fm, matter polarization dominates, and one can observe qualitatively new features.

6.1 Rho-meson exchange

On the left upper panel of Fig. 9, we show the contribution of one-rho meson exchange to the central component of the potential. We compare the results obtained for the in-medium potential at $p_F/m = 0.4$ (corresponding to a density $\rho = 2.37\rho_0$) to the free-space potential (dotted curve), which was calculated setting $p_F = 0$. Vacuum polarization effects are kept in all cases. We made the calculation for three types of renormalization schemes, one of the first "increasing rho mass" class (scheme 1 with parameter set 1B), and two of the "decreasing rho mass" class (scheme 5=Shiomi-Hatsuda with Machleidt's Bonn B parameters and scheme 3=ours with parameter set 3A).

From this comparison, we observe that the use of a screened interaction in matter can bring appreciable modifications to the potential described by the exchange of free mesons in the vacuum. In particular, in the long-range region, the interaction is qualitatively different from vacuum. Instead of the usual exponential damping, at non-zero density the potential becomes oscillatory due to the presence of *Friedel and Yukawa oscillations*. This behavior is obtained whatever renormalization procedure is chosen.

Friedel oscillations arise because the analytically-continued matter polarization shows branch cuts starting at $q = \pm 2p_F$ in the complex q-plane. This phenomenon was first discovered for a QED plasma [6] and was also evidenced in the case of a QCD plasma [8]. The corresponding analysis for a nucleon plasma in different models was performed in [10, 12, 11]. On the other hand, Yukawa oscillations appear when the analytically-continued boson propagator has a pole (in the complex q-plane) away from the real and imaginary axis. Such a phenomenon has been found so far for a nucleon plasma in the one-pion exchange approximation, and for a quark-gluon plasma when one-gluon exchange is considered [59]. In order to separate Friedel from Yukawa effects for rho mesons, one needs to perform the analytical continuation of the meson propagator and to study the evolution of the Yukawa pole as density and temperature evolves. This will be the subject of a future work.

These oscillating phenomena can have consequences if one goes beyond the Hartree approximation, by including the polarization contribution into the ground-state energy. In the case of Friedel oscillations, it has been found that a periodic-density configuration, with period equal to the characteristic period of Friedel oscillations, has a lower energy than a constant-density configuration [60]. This can be interpreted as a transition to a spatially-structured configuration.

For a fixed renormalization scheme, we obtained that the repulsive core extends farther when density increases. On the other hand, for a given value of the density, the first minimum occurs earlier for renormalization

---

[6]Preliminary studies indicate however that this would spoil the behavior of the σ and π effective masses [30].

schemes of the first "increasing rho mass" class than for schemes of the second class. In the long-range zone, the period of oscillation is seen to be the same for all renormalization schemes, and depends only on the density, as expected from the physical origin of Friedel oscillations.

Matter polarization dominates the potential qualitative features at large distances. The choice of a renormalization scheme can, however, introduce some quantitative changes on these features. The amplitude of the oscillations depends indirectly on the renormalization scheme. For example, to each scheme, there corresponds a parameter set with different values of the couplings and cutoffs. The amplitude can be enhanced by the presence of a dip in the dispersion relation of the transverse modes, indicating the proximity of a zero sound mode, even when no pole actually appears. On the other hand we found that the appearance of such a branch depends on the renormalization procedure, the second class of renormalization schemes being less liable to the appearance of zero sound modes. Nevertheless, we would like to stress that the oscillations themselves are not a consequence of possible zero sound modes, since we found them also in the renormalization scheme of Sarkar, where no zero sound was obtained even for extreme choices of the parameters and density.

Similar features can be observed in the remaining components (spin-spin, tensor and spin-orbit) of the potential. They are plotted in the three remaining panels of Fig. 9). They all show an oscillatory behavior. In all cases, the amplitude of oscillations increases with density.

6.2   Combined-meson potential

We will now present some results which are obtained by adding the contribution of the $\sigma + \omega$ sector and the π exchange to the potential given above[7]. For the central component there is no pion contribution, and one has :

$$V_c(r) = V_c^{\sigma+\omega}(r) + V_c^\rho(r) \tag{58}$$

The result is plotted in Fig. 10 in vacuum (solid curve) and at finite densities $p_F = 0.3, 0.4, 0.5$ (dashed, dot-dashed and dotted lines respectively). In this figure the renormalization scheme 1 was chosen with parameter set B. The free-space potential (which includes vacuum polarization with on-shell renormalization, scheme 1) has a potential well with a minimum at $r \sim 1.5$ fm. At finite density, the position of the first minimum is displaced towards shorter distances: at saturation density ($p_F = 0.3$) it corresponds to $r \sim 1.25$ fm, whereas for $p_F = 0.5$ it is located at $r \sim 0.95$ fm. There also appear secondary minima which depth can be significant. In the example chosen, at $p_F = 0.5$ ($\rho = 4.63 \rho_0$), the second minimum is situated at $r \sim 2.1 fm$ with a depth of -8 MeV. The right panel of Fig. 10 focusses on the long-range oscillatory behavior. Here it can be seen that the period of the oscillation decreases and its amplitude increases with increasing density.

We also studied the spin-spin, tensor and spin-orbit components of the potential. The results are not shown here; basically the same features as already mentioned in the case of the rho component were observed.

7   Mechanisms reducing the amplitude of oscillations

In this section we discuss the mechanisms which could suppress the oscillations found in the in-medium NN potential.

We will first investigate the contribution of meson loops to the ρ-meson self energy. As is well known, the spectral function of the rho meson acquires an important contribution of the $\rho\pi\pi$ loop (see *eg.* [44]). A meson with a mass distribution, such as the σ or the ρ, could smear away some features in the potential by merging contributions with different ranges. As we will see, the effect on the potential is negligible. For consequences on the dilepton production in the vector dominance model, we refer the reader to the vast litterature devoted to this subject (see *eg.* [44, 45, 61, 62] and references therein).

A second and more effective mechanism is the rounding off of the edge of the Fermi momentum distribution function introduced by short-range correlations or by a finite temperature. This will be investigated in the second part of this section.

7.1   Meson loops

We have up to now studied the contribution of nucleon-hole loops to the ρ meson polarization. On the other hand, the ρ meson also couples to the pion, a fact which is at the origin of the decay width of the ρ meson. Let

---

[7]The contribution from δ and η mesons is not included here since they introduce only a small modification to the vacuum potential of [1]

us add to the Lagrangian a piece

$$\mathcal{L}_{\rho\pi\pi} = g_{\rho\pi\pi}(\partial^\mu \vec{\pi} \times \vec{\pi}).\vec{\rho}_\mu + \frac{1}{2}g_{\rho\pi\pi}^2(\vec{\rho}^\mu \times \vec{\pi}).(\vec{\rho}_\mu \times \vec{\pi}) \tag{59}$$

At the first order of the linear expansion method of [24], meson loops do not appear. It would be necessary to go to higher orders in the cluster expansion, so that meson-meson correlators appear. We would like here to estimate the correction brought by the $\rho\pi\pi$ polarization loop. From Green function techniques, one obtains [29, 44, 63]

$$\Pi_{\rho\pi\pi} = ig_{\rho\pi\pi}^2 \int \frac{d^4p}{(2\pi)^4}(2p-k)^\mu(2p-k)^\nu D_\pi(p)D_\pi(p-k) - 2ig_{\rho\pi\pi}^2 \int \frac{d^4p}{(2\pi)^4}g^{\mu\nu}D_\pi(p) \tag{60}$$

In general, the pion propagator also includes medium effects. In order to keep things simple however, we will keep here the free pion propagator $D_\pi^0(k) = 1/(k^2 - \mu_\pi^2 + i\epsilon)$.

The coupling constant $g_{\rho\pi\pi}$ is determined by fixing the imaginary part of the polarization on the ρ meson mass shell and in the rest frame to its experimental value

$$\Gamma_{\rho\pi\pi} = -\frac{1}{\mu_\rho}\mathcal{I}m\Pi_{\rho\pi\pi}(\omega = \mu_\rho, \vec{q} = 0) = \frac{g_{\rho\pi\pi}^2}{48\pi\mu_\rho^2}(\mu_\rho^2 - 4\mu_\pi^2)^{3/2} \tag{61}$$

Putting $\Gamma_{\rho\pi\pi} \simeq 151.5$ MeV, one finds $g_{\rho\pi\pi}^2/(4\pi) \simeq 2.9$ The real part of the polarization can be expressed in terms of the divergent integrals (40)

$$\mathcal{R}e\,\Pi_{\rho\pi\pi}^{\mu\nu} = -\frac{2}{3}\frac{g_{\rho\pi\pi}^2}{(2\pi)^2}\left[2\mathcal{I}_1 + k^2(\mu_\pi^2 - \frac{k^2}{4})\mathcal{I}_2\right]\left(g^{\mu\nu} - \frac{k^\mu k^\nu}{k^2}\right) \tag{62}$$

After performing dimensional regularization,

$$\mathcal{R}e\,\Pi_{\rho\pi\pi}^{\mu\nu} = -\frac{2}{3}\frac{g_{\rho\pi\pi}^2}{(2\pi)^2}\left(g^{\mu\nu} - \frac{k^\mu k^\nu}{k^2}\right)\left[(\frac{k^2}{4} - \mu_\pi^2)\theta(k^2, \mu_\pi^2) - \frac{k^2}{\epsilon}\right] \tag{63}$$

The infinity is cancelled by a counterterm of the form $A_{\rho\pi\pi}R^{\mu\nu}R_{\mu\nu}$, that is to say, the renormalization proceeds exactly as in the unambiguous case of the NN loop contribution to the ω meson. The finite result is:

$$\mathcal{R}e\,\Pi_{\rho\pi\pi}^{\mu\nu} = -\frac{2}{3}\frac{g_{\rho\pi\pi}^2}{(2\pi)^2}\left(g^{\mu\nu} - \frac{k^\mu k^\nu}{k^2}\right)\left[\frac{\mu_\pi^2}{\mu_\rho^2}(\mu_\rho^2 - k^2)\left(1 - \theta(\mu_\rho^2, \mu_\pi^2)\right) + (\mu_\pi^2 - \frac{k^2}{4})\left(\theta(\mu_\rho^2, \mu_\pi^2) - \theta(k^2, \mu_\pi^2)\right)\right] \tag{64}$$

The imaginary part is given by

$$\mathcal{I}m\,\Pi_{\rho\pi\pi}^{\mu\nu} = \frac{g_{\rho\pi\pi}^2}{48\pi}k^2\left(1 - 4\frac{\mu_\pi^2}{\mu_\rho^2}\right)^{3/2}\theta(k^2 - 4\mu_\pi^2) \tag{65}$$

In the calculation of the potential, the imaginary part will not contribute since the polarizations entering the formulae are to be taken at $\omega = 0$ while the imaginary part should be an odd function of ω so that the Onsager relations be fulfilled. The real part of the polarization yields a small shift to the dispersion relation. We have checked that its effect on the potential is negligible. At the level of approximation considered here, the shift is q-dependent but does not depend on thermodynamical conditions. It would if we introduced the modification of the pion propagator by $N\Delta$ loops or a bath of thermal pions (see *eg.* [61]).

7.2 Effect of short range correlations

A second mechanism which can attenuate the long range oscillatory behavior of the in-medium potential is the rounding-off of the momentum distribution by short-range correlations of the Brueckner type. As commented in the introduction, a fully consistent calculation at the level of parquet approximation would be required. Here, in order to estimate the order of magnitude of this effect, we will simply introduce such a momentum distribution instead of the Fermi-Dirac one in the calculation of the polarizations.

Among the results available in the literature we chose two: a non relativistic Brueckner-Hartree-Fock calculation of Baldo *et al.* starting from a separable Paris interaction [64], and a Dirac-Brueckner-Hartree-Fock

16

calculation by de Jong and Malfliet [65]. It seems more appropriate to use the calculation of de Jong and Malfliet since it is fully relativistic and was obtained starting from the Bonn potential. Moreover, these authors checked explicitly that the thermodynamical consistency be optimally fulfilled. On the other hand, comparison with experimental data seems to favor the larger depletion and smaller discontinuity found in nonrelativistic calculations such as that of Baldo *et al.*, so that we also present results with this distribution.

We found that the data published by de Jong and Malfliet was well reproduced by the following fit at saturation density:

$$
F_{DBHF}(k) = \begin{cases} 0.91 - 0.055 \left(\dfrac{k}{p_F}\right) - 0.07 \left(1 - \dfrac{k}{p_F}\right) \log\left(1 - \dfrac{k}{p_F}\right) & \text{if } k < p_F \\[2mm] \dfrac{0.035}{k/p_F - 0.94} \ \exp\left(-1.2\dfrac{k}{p_F}\right) & \text{if } p_F < k < 1.5 p_F \\[2mm] 0.3693 \ \exp\left(-2.4\dfrac{k}{p_F}\right) & \text{if } k > 1.5 p_F \end{cases} \tag{66}
$$

For the data of Baldo *et al.*, we used

$$
F_{NRBHF}(k) = \begin{cases} 0.79 - 0.13 \left(\dfrac{k}{p_F}\right) - 0.19 \left(1. - \dfrac{k}{p_F}\right) \log\left(1 - \dfrac{k}{p_F}\right) & \text{if } k < p_F \\[2mm] 16. \ \exp\left(-4.5\dfrac{k}{p_F}\right) & \text{if } p_F < k < 1.5 p_F \\[2mm] 0.2127 \ \exp\left(-1.6\dfrac{k}{p_F}\right) & \text{if } k > 1.5 p_F \end{cases} \tag{67}
$$

We now calculate the polarizations at vanishing temperature as

$$
\Pi_{BHF}(k) = \int_0^\infty d^3p \ \frac{\partial \Pi_{FD}^{(T=0)}(k,p)}{\partial p} \ F_{BHF}(p) \tag{68}
$$

where $\Pi_{FD}^{(T=0)}$ is the polarization which would have been obtained with a Fermi Dirac step function $\theta(p_F - p)$ and is given in Appendix A. Next we introduce these polarizations in the expression of the potentials given in Appendix C. Figure 11 compares the central potential as obtained with parameter set 1B at vanishing temperature and saturation density for the Fermi-Dirac momentum distribution (dashed line), the relativistic DBHF distribution of de Jong and Malfliet (full line) and the nonrelativistic BHF distribution of Baldo *et al.* (dotted line). It is seen that the oscillations are damped by Brueckner correlations as was to be expected. The effect is however not very severe and the oscillations persist.

7.3 Effect of finite temperature

A similar damping of the oscillations is produced by a non-vanishing temperature. We found that the Brueckner modification of the momentum distribution had the same effect as a temperature of ~ 10 MeV with a Fermi-Dirac distribution. It can be seen on Figure 12 that Friedel oscillations are rather robust against temperature and are not washed out for temperatures as high as 30 MeV.

As a by-product, we obtained the behavior of the ρ effective mass as a function of temperature for all renormalization schemes. At saturation density, it was found that μ_{eff} (calculated as in section 5.3) slightly decreases with temperature for renormalization schemes of the first class 1, 2 and 6, whereas it slightly increases for renormalization schemes of the second class 3, 4 and 5. At four times the saturation density, μ_{eff} was found to decrease for all renormalization schemes. The results are well described by a linear law for temperatures $T \in [0 - 100]$ MeV:

$$
\frac{\mu_{eff}}{\mu_\rho}(\rho, T) = \frac{\mu_{eff}}{\mu_\rho}(\rho, 0) \left(1 - a\frac{T}{m}\right) \tag{69}
$$

with

$a = 0.4$	for $\rho = \rho_0$	renorm. scheme=		1 or 2
$a = 0.35$	" "	"	"	6
$a = -0.12$	" "	"	"	3, 4 or 5
$a = 1.5$	for $\rho = 4\,\rho_0$	renorm. scheme=		1 or 2
$a = 0.8$	" "	"	"	6
$a = 0.55$	" "	"	"	3, 4 or 5

8   Discussion and Conclusions

In this paper we have discussed RPA effects on the nucleon-nucleon potential obtained within the one-boson exchange approximation in symmetric nuclear matter at zero temperature. The model we used for our calculations includes σ , ω , π and ρ mesons interacting with nucleons via Yukawa couplings. The Wigner function technique and linear response analysis were used to obtain the meson propagation in medium. The lowest order of this scheme is the mean-field approximation. When vacuum effects are properly renormalized, it becomes the Hartree approximation. The next order of this approximation has been shown to be equivalent to Green's function calculations of the meson propagators at one-loop order[23].

In our calculations, medium effects appear in two ways. First, in the nucleon legs of the one-boson exchange diagram the nucleon effective mass appears. Secondly, the meson propagators are calculated including nucleon-hole loops and vacuum polarization effects.

It is legitimate to ask whether one should consider other loops involving mesons or resonances [54]. Only a brief discussion concerning pion-pion loops was given, since several thorough studies exist in the litterature [44, 63, 61]. Loops involving resonances can be expected to have a smaller but sizeable contribution of similar characteristics to the nucleon loop taken into account in this work. A serious study with renormalization would, however, go beyond the scope of this paper.

In symmetric nuclear matter, rho mesons decouple from other mesons. Therefore, it is possible to study one-ρ exchange alone and simply add the contribution of σ , ω and π to the nucleon-nucleon potential at the end. We have first studied the *dispersion relations* which describe the propagation of rho-mesons in matter as density changes. One observes the presence of two types of branches : a *normal branch*, which is the analogous of the free-space mass-shell condition, and several *heavy-meson branches*. The latter appear as a consequence of vacuum effects, in all the QHD meson models that have been investigated [23, 24, 66]. Here, due to the derivative coupling of the rho-mesons to the nucleons, the Lagrangian is non-renormalizable. Yet, it is possible to extract a finite contribution from the vacuum at each order in the cluster expansion[8]. This procedure, however, contains some arbitrariness in the case of non-renormalizable Lagrangians.

In view of this, we have compared the results arising from two different classes of renormalization schemes. The first one is analogous to the one usually employed in previous works [25, 28, 10] and is designed to remove, as far as possible, the spurious new couplings to the sigma field which have to be introduced in the counterterm Lagrangian. The renormalization procedure suggested in [27] has also been used for comparison. We found that it belongs to a second class of procedures, where the new couplings to the sigma field are not minimized, but instead the original structure of the expression of the vacuum contribution is preserved.

By using the first scheme, we find that the effective mass of rho-mesons grows with density, a feature which is disfavored by most of present theoretical approaches and by the interpretation of dilepton production data in heavy-ion collisions. The second method gives the opposite behavior : the in-medium rho-meson mass drops as density grows, more in agreement with present ideas. However, it is recognized that large uncertainties are contained both in the theoretical calculations [46, 37] and the analysis of experiments mentioned above [52, 42, 62]. We have kept for these reasons these two schemes in our calculations.

Next, we investigated the RPA nucleon-nucleon potential obtained by the exchange of one rho meson. At short and intermediate distances, it shows a repulsive behavior. In the long-range it contains new qualitative features, as compared to the free-space potential. It becomes oscillatory, with an amplitude which decreases with distance, due to the combination of Yukawa-like and Friedel oscillations. The appearance of this oscillatory behavior might give rise to a new phase of dense matter, characterized by a spatially structured density distribution. We have verified that the qualitative features within this distance range are not sensitive to the renormalization scheme used. One then expects that they are to be found in other models describing rho-meson propagation in dense nuclear matter.

---

[8]We use the word *renormalization* in a wide sense to describe this procedure, in spite of the non-renormalizability of the model.

When other mesons are added into the potential, we find a similar behavior. The potential is repulsive at short distances and attractive at intermediate distances. In the long-range, $r \geq 2$ fm, we find again an oscillatory behavior in all components of the potential, with the same origin as above. The amplitude of these oscillations increase with density.

The robustness of these oscillations against several possible damping mechanisms has been tested. We first discussed the influence of pion-pion loops. In the *spacelike* zone explored by the potential, we found that it should not have a decisive impact on the results presented. This does not enter in contradiction with the large body of publications for which the spectral function is needed in the *timelike* region.

We also investigated the amount of smoothing of the Friedel oscillations to be expected from modifications to the Fermi surface. In particular, we discussed the effect of the temperature and short-range correlations. We performed a calculation with a momentum distribution rounded off by short range correlations of the Brueckner type, and found they have the same consequences as a temperature of about 10 MeV, namely, that the oscillations experiment a moderate damping, and are seen discernible. They only disappear for temperatures higher than 30 MeV.

One has to exert some care when considering the applicability to the above results to actual nuclear-matter calculations. The RPA summation concerns only a class of many-body diagrams, so that the addition of different diagrams, such as ladder diagrams, might modify our results (one would expect, however, that in the long-distance range the RPA results would hold). The obtained potential can not be used naively to perform more elaborated calculations (such as ladder resummation) since it would result in double counting of diagrams. Our results rather have to be interpreted as an indication of a new qualitative effect that one might find.

To summarize, screening effects can appreciably modify the nature of nuclear interactions in a medium. Vacuum effects also compete to modify the interaction, so that it is important to design a procedure which incorporates them in a consistent way. However, the appearance of singular behaviors, as Friedel and Yukawa-like oscillations seems to be a rather general property of the nuclear interaction.

Acknowledgments

Appendix A: Polarization, matter part

We give here the complete formulae for the matter part of the rho-meson polarization tensor in symmetric nuclear matter. The vacuum contribution is given in Appendix B. This tensor can be written as :

$$\Pi_\rho^{\mu\nu}(k) \;=\; -\int d^4p \; I^{\mu\nu}(p,k) \; J(p,k) \tag{1}$$

where

$$
\begin{aligned}
I^{\mu\nu}(p,k) \;=\; & \; g_\rho^2 \left[\left(4\,M^2 + k^2 - 4\,p^2\right) g^{\mu\nu} - 2\,k^\mu k^\nu + 8\,p^\mu p^\nu \right] \\
& + \left(\frac{f_\rho}{2m}\right)^2 \left[\left(4\,M^2 k^2 + k^4 + 4\,p^2 k^2 - 8\,(p.k)^2\right) g^{\mu\nu} - \left(k^2 + 4\,M^2 - 4\,p^2\right) k^\mu k^\nu \right. \\
& \hspace{3em} \left. + 8\,(p.k)\left(k^\mu p^\nu + p^\mu k^\nu\right) - 8\,k^2 p^\mu p^\nu \right] \\
& + \left(\frac{f_\rho}{2m}\right) g_\rho \left[8\,M\left(k^2 g^{\mu\nu} - k^\mu k^\nu\right) \right]
\end{aligned}
\tag{2}
$$

In this equation, M is the nucleon effective mass, and m its free mass. We have introduced :

$$J(p,k) = \frac{f(p+k/2) - f(p-k/2)}{k \cdot p} \tag{3}$$

The nucleon distribution functions, as they arise from the relativistic Hartree approximation, are the same for protons and neutrons (in symmetric nuclear matter). They are given by

$$f(p) = \frac{\delta(p^2 - M^2)}{(2\pi)^3} \left[\frac{H(p^0)}{e^{\beta\,(p^0 - \mu_{eff})} + 1} + \frac{H(p^0)}{e^{\beta\,(p^0 + \mu_{eff})} + 1} - H(-p^0) \right] \tag{4}$$

Here, $\mu_{eff} = \mu + g_\omega <\omega^0>$ is the nucleon effective chemical potential, μ is the true chemical potential and β is the inverse temperature. The time-like mean field value $<\omega^0>$ of the ω meson is also calculated within the Hartree approximation. Finally, $H(x)$ is the Heaviside step function.

At zero temperature, it is possible to perform the integrals in Eq. (1) analytically. Moreover, in order to obtain the nucleon-nucleon potential, within the approximations discussed in this work, we only need to calculate the matter polarization on the $k^0 = 0$ axis. In this case, one gets more compact expressions. We give here these formulae. By defining $q = |\vec{k}|$, $\varepsilon = \sqrt{M^2 + (q/2)^2}$ and the nucleon Fermi energy $E_F = \sqrt{M^2 + p_F^2}$, we can introduce the notations

$$A(q) = \frac{q - 2p_F}{q + 2p_F} , \quad B(q) = \frac{q E_F + 2 p_F \varepsilon}{q E_F - 2 p_F \varepsilon} \tag{5}$$

One finds, after some algebra:

$$
\begin{aligned}
\Pi_{\rho L}(0, q) &= \Pi_\rho^{00}(0, q) \\
&= \frac{g_\rho^2}{\pi^2}\left[-\frac{4}{3}E_F p_F + \frac{q^2}{3}\ln\left(\frac{E_F + p_F}{M}\right) - \frac{E_F}{2}\left(q - \frac{4}{3}\frac{E_F^2}{q}\right)\ln A(q) - \frac{\varepsilon}{2}\left(q - \frac{4}{3}\frac{\varepsilon^2}{q}\right)\ln B(q)\right] \\
&\quad + \left(\frac{f_\rho}{2m}\right)^2\frac{q^2}{\pi^2}\left[-\frac{1}{3}E_F p_F + \left(M^2 - \frac{q^2}{6}\right)\ln\left(\frac{E_F + p_F}{M}\right) + 2\frac{E_F}{q}\left(\frac{E_F^2}{3} - M^2\right)\ln A(q)\right. \\
&\quad \left. + 2\frac{\varepsilon}{q}\left(\frac{\varepsilon^2}{3} - M^2\right)\ln B(q)\right] \\
&\quad + \left(\frac{f_\rho}{2m}\right)g_\rho\frac{2Mq^2}{\pi^2}\left[\ln\left(\frac{E_F + p_F}{M}\right) - \frac{E_F}{q}\ln A(q) - \frac{\varepsilon}{q}\ln B(q)\right]
\end{aligned}
\tag{6}
$$

$$\tag{7}$$

for the longitudinal part, and

$$
\begin{aligned}
\Pi_{\rho T}(0, q) &= -\Pi_\rho^{11}(0, q) \\
&= -\frac{g_\rho^2}{2\pi^2}\left[\frac{2}{3}E_F p_F - \frac{2}{3}q^2\ln\left(\frac{E_F + p_F}{M}\right) - E_F\left(2\frac{\varepsilon^2}{q} - \frac{2}{3}\frac{E_F^2}{q} - q\right)\ln A(q) - \varepsilon\left(\frac{4}{3}\frac{\varepsilon^2}{q} - q\right)\ln B(q)\right] \\
&\quad - \left(\frac{f_\rho}{2m}\right)^2\frac{q^2}{2\pi^2}\left[-\frac{4}{3}E_F p_F + \left(\frac{q^2}{3} - 2M^2\right)\ln\left(\frac{E_F + p_F}{M}\right) + 2\frac{E_F}{q}\left(\frac{E_F^2}{3} + \varepsilon^2\right)\ln A(q)\right. \\
&\quad \left. + \frac{8}{3}\frac{\varepsilon^3}{q}\ln B(q)\right] \\
&\quad + \left(\frac{f_\rho}{2m}\right)g_\rho\frac{2Mq^2}{\pi^2}\left[\ln\left(\frac{E_F + p_F}{M}\right) - \frac{E_F}{q}\ln A(q) - \frac{\varepsilon}{q}\ln B(q)\right]
\end{aligned}
\tag{8}
$$

for the transverse part.

Appendix B: Polarization, vacuum contribution

The vacuum contribution arises from the $-H(-p_0)$ term in the distribution function $f(p)$. This contribution is divergent and has to be renormalized. After performing a dimensional regularization and subtracting the appropriate counterterms, we obtained in section III a finite expression for the vacuum polarization:

$$
\begin{aligned}
\Pi_{\rho\ vac}^{\mu\nu} &= \left\{\frac{g_\rho^2}{3\pi^2}\left[\ln\left(\frac{M}{m}\right) + \theta(k^2, M^2) + \frac{2M^2}{k^2}\left(\theta(k^2, M^2) - 1\right)\right]\right. \\
&\quad + \left(\frac{f_\rho}{2m}\right)^2\frac{1}{6\pi^2}\left[6M^2\ln\left(\frac{M}{m}\right) + 8M^2\theta(k^2, M^2) + k^2\left(\ln\left(\frac{M}{m}\right) + \theta(k^2, M^2)\right)\right] \\
&\quad + \frac{2}{\pi^2}\left(\frac{f_\rho}{2m}\right)g_\rho M\left[\ln\left(\frac{M}{m}\right) + \theta(k^2, M^2)\right]
\end{aligned}
$$

$$+\alpha + \beta\frac{(m-M)}{g_\sigma} + \gamma\frac{(m-M)^2}{g_\sigma^2} + \delta k^2\bigg\} \left\{k^2 g^{\mu\nu} - k^\mu k^\nu\right\} \tag{1}$$

with the function

$$\theta(k^2, M^2) \;=\; \theta(y) \;\equiv\; y\int_0^\infty \frac{dx}{\left[(x^2 + y).\sqrt{(x^2 + 1)}\right]} \tag{2}$$

where $y \equiv 1 - k^2/(4M^2)$.

The choice of conditions to be imposed on the polarization to determine the finite constants α, β, γ, δ determine various renormalization schemes.

In order to shorten the notations, we define

$$\theta_\rho \;=\; \theta(\mu_\rho^2, m^2)\,, \qquad \theta_{\rho m} \;=\; \frac{\partial\theta(k^2, M^2)}{\partial M}$$

$$\theta_{\rho k} \;=\; \frac{\partial\theta(k^2, M^2)}{\partial k^2}\,, \qquad \theta_{\rho mm} \;=\; \frac{\partial^2\theta(k^2, M^2)}{\partial M^2} \tag{3}$$

All these derivatives are to be evaluated in the point $k^2 = \mu_\rho^2$, $M = m$.

We will note $\theta = \theta(k^2, M^2)$. Finally, we will work in units of the nucleon free mass, *i.e.* we set $m = 1$ in all expressions given in this Appendix.

Scheme 1

When the full set of conditions (47 – 50) is applied to the total regularized vacuum polarization of the ρ meson, the following expression is obtained

$$\begin{aligned}
\Pi^{\mu\nu}_{\rho\ vac(1)} \;=\; \Bigg\{ &\frac{g_\rho^2}{3\pi^2}\bigg[\ln M + \theta + \frac{2M^2}{k^2}(\theta - 1) - \frac{1}{\mu_\rho^2}\left((2 + \mu_\rho^2)\theta_\rho - 2\right) \\
&+ (1 - M)\left(1 + \theta_{\rho m} + \frac{4}{\mu_\rho^2}(\theta_\rho - 1) + \frac{2}{\mu_\rho^2}\theta_{\rho m}\right) \\
&- \frac{1}{2}(1 - M)^2\left(-1 + \theta_{\rho mm} + \frac{4}{\mu_\rho^2}(\theta_\rho - 1) + \frac{8}{\mu_\rho^2}\theta_{\rho m} + \frac{2}{\mu_\rho^2}\theta_{\rho mm}\right) \\
&- (k^2 - \mu_\rho^2)\left(1 + \frac{2}{\mu_\rho^2}\theta_{\rho k} - \frac{2}{\mu_\rho^4}(\theta_\rho - 1)\right)\bigg] \\
&+ \left(\frac{f_\rho}{2m}\right)^2\frac{1}{6\pi^2}\bigg[6M^2\ln M + 8M^2\theta + k^2(\ln M + \theta) - (8 + \mu_\rho^2)\theta_\rho \\
&+ (1 - M)\left(6 + 16\,\theta_\rho + 8\,\theta_{\rho m} + \mu_\rho^2(1 + \theta_{\rho m})\right) \\
&- \frac{1}{2}(1 - M)^2\left(18 + 16\,\theta_\rho + 32\,\theta_{\rho m} + 8\theta_{\rho mm} + \mu_\rho^2(-1 + \theta_{\rho mm})\right) \\
&- (k^2 - \mu_\rho^2)\left((8 + \mu_\rho^2)\theta_{\rho k} + \theta_\rho\right)\bigg] \\
&+ \frac{2}{\pi^2}\left(\frac{f_\rho}{2m}\right)g_\rho\bigg[M(\ln M + \theta) - \theta_\rho + (1 - M)(\theta_\rho + 1 + \theta_{\rho m}) \\
&- \frac{1}{2}(1 - M)^2(1 + 2\,\theta_{\rho m} + \theta_{\rho mm}) - (k^2 - \mu_\rho^2)\,\theta_{\rho k}\bigg]\Bigg\}\left\{k^2 g^{\mu\nu} - k^\mu k^\nu\right\} \tag{4}
\end{aligned}$$

Scheme 2

The former scheme has the drawback that we do not recover the expression of the vacuum polarization of the ω meson when we take the limit $f_\rho \to 0$ and replace g_ρ by g_ω. The reason is that the structure of the infinities is not the same for the different couplings. By renormalizing all contributions together we are in fact introducing spurious counterterms where they need not be. For example, in the $(f_\rho/2m)^2$ contribution we have both M^2/ϵ and k^2/ϵ, needing all sets of counterterms to cancel them, whereas in the g_ρ^2 contribution we have a

21

$1/\epsilon$ which requires only the $A\,\vec{R}^{\mu\nu}\cdot\vec{R}_{\mu\nu}$ counterterm. This can easily be cured by splitting the counterterms as follows $A = A_{gg} + A_{fg} + A_{ff}$, $B = B_{fg} + B_{ff}$, $C = C_{ff}$, $D = D_{ff}$, (where A_{fg}, B_{fg} mean terms proportional to $g_\rho\, f_\rho$, and so on) and renormalized separately each contribution. We obtain

$$
\begin{aligned}
\Pi^{\mu\nu}_{\rho\ vac(2)} \;=\; & \left\{ \frac{g_\rho^2}{3\pi^2}\left[\ln M + \theta + \frac{2M^2}{k^2}(\theta - 1) - \frac{1}{\mu_\rho^2}\left((2 + \mu_\rho^2)\,\theta_\rho - 2 \right) \right] \right. \\
& + \left(\frac{f_\rho}{2m}\right)^2 \frac{1}{6\pi^2}\left[6M^2 \ln M + 8M^2\theta + k^2(\ln M + \theta) - (8 + \mu_\rho^2)\,\theta_\rho \right. \\
& \qquad\qquad + (1 - M)\left(6 + 16\,\theta_\rho + 8\,\theta_{\rho m} + \mu_\rho^2(1 + \theta_{\rho m}) \right) \\
& \qquad\qquad - \frac{1}{2}(1 - M)^2\left(18 + 16\,\theta_\rho + 32\,\theta_{\rho m} + 8\,\theta_{\rho m m} + \mu_\rho^2(-1 + \theta_{\rho m m}) \right) \\
& \qquad\qquad \left. - (k^2 - \mu_\rho^2)\left((8 + \mu_\rho^2)\,\theta_{\rho k} + \theta_\rho \right) \right] \\
& \left. + \frac{2}{\pi^2}\left(\frac{f_\rho}{2m}\right) g_\rho\left[M(\ln M + \theta) - \theta_\rho + (1 - M)(\theta_\rho + 1 + \theta_{\rho m}) \right] \right\} \{ k^2 g^{\mu\nu} - k^\mu k^\nu \}
\end{aligned}
\tag{5}
$$

Scheme 3

We observe that there appear infinities which can be written as depending on M (rather than on σ), as for example M^2/ϵ. After absorbing the infinities, the finite part of the counterterms is $a_{ff} + b_{ff}\sigma + c_{ff}\sigma^2$. The constants a_{ff}, b_{ff}, c_{ff} which are calculated by imposing the conditions (47) and (49,50) cannot be cast any more in a form proportional to M^2. One would like to require that the M^2 structure be preserved by dropping conditions (49,50). Proceeding in this way, we obtain

$$
\begin{aligned}
\Pi^{\mu\nu}_{\rho\ vac(3)} \;=\; & \left\{ \frac{g_\rho^2}{3\pi^2}\left[\ln M + \theta + \frac{2M^2}{k^2}(\theta - 1) - \frac{1}{\mu_\rho^2}\left((2 + \mu_\rho^2)\,\theta_\rho - 2 \right) \right] \right. \\
& + \left(\frac{f_\rho}{2m}\right)^2 \frac{1}{6\pi^2}\left[6M^2 \ln M + 8M^2\theta + k^2(\ln M + \theta) - (8 + \mu_\rho^2)\,\theta_\rho \right. \\
& \qquad \left. - (k^2 - \mu_\rho^2)\left((8 + \mu_\rho^2)\,\theta_{\rho k} + \theta_\rho \right) + (M^2 - 1)\left(\mu_\rho^2(8 + \mu_\rho^2)\,\theta_{\rho k} - 8\theta_\rho \right) \right] \\
& \left. + \frac{2}{\pi^2}\left(\frac{f_\rho}{2m}\right) g_\rho\left[M(\ln M + \theta - \theta_\rho) \right] \right\} \{ k^2 g^{\mu\nu} - k^\mu k^\nu \}
\end{aligned}
\tag{6}
$$

Scheme 4

We show in this section and the next how the results of Shiomi and Hatsuda [27] and Sarkar *et al.* [29] can be recovered. We first observe that the regularized vacuum polarization can be written as follows:

$$
\Pi^{\mu\nu}_{\rho\ vac} = \left\{ g_\rho^2 \mathcal{A} + \left(\frac{f_\rho}{2m}\right)^2\left[\frac{k^2}{2}\mathcal{A} + \frac{M^2}{2}\mathcal{B} \right] + g_\rho\left(\frac{f_\rho}{2m}\right) M\mathcal{B} \right\}\left(g^{\mu\nu} - \frac{k^\mu k^\nu}{k^2} \right)
\tag{7}
$$

with

$$
\begin{aligned}
\mathcal{A} \;&=\; \frac{2}{(2\pi)^3}\frac{1}{k^2}\left[-16\mathcal{I}_1/3 - 2/3k^2(2M^2 + k^2)\mathcal{I}_2 \right] \\
\mathcal{B} \;&=\; \frac{2}{(2\pi)^3}\left[-4k^2\mathcal{I}_2 \right]
\end{aligned}
$$

If we now impose that this structure be kept after the renormalization, with $\mathcal{A}$ and $\mathcal{B}$ substituted by finite $\widetilde{\mathcal{A}}$ and $\widetilde{\mathcal{B}}$ after extracting the infinities, we can determine the constants by imposing that $\widetilde{\mathcal{A}}$ and $\widetilde{\mathcal{B}}$ vanish on the mass shell. By so doing we obtain

$$\widetilde{\mathcal{A}} = \frac{1}{3\pi^2}\left[\ln(M) + \theta + \frac{2M^2}{k^2}(\theta - 1) - \frac{1}{\mu_\rho^2}\left((2 + \mu_\rho^2)\theta_\rho - 2\right)\right]$$

$$\widetilde{\mathcal{B}} = \frac{2k^2}{\pi^2}\left[\ln(M) + \theta - \theta_\rho\right]$$

and

$$
\begin{aligned}
\Pi_{\rho\ vac(4)}^{\mu\nu} = {}& \left\{ \frac{g_\rho^2}{3\pi^2}\left[\ln M + \theta + \frac{2M^2}{k^2}(\theta - 1) - \frac{1}{\mu_\rho^2}\left((2 + \mu_\rho^2)\theta_\rho - 2\right)\right] \right. \\
& + \left(\frac{f_\rho}{2m}\right)^2 \frac{1}{6\pi^2}\left[6M^2\ln M + 8M^2\theta + k^2(\ln M + \theta) - 2M^2 - 6M^2\theta_\rho \right. \\
& \qquad \left. - \frac{k^2}{\mu_\rho^2}\left((2 + \mu_\rho^2)\theta_\rho - 2\right)\right] \\
& \left. + \frac{2}{\pi^2}\left(\frac{f_\rho}{2m}\right)g_\rho\left[M(\ln M + \theta - \theta_\rho)\right]\right\}\left\{k^2 g^{\mu\nu} - k^\mu k^\nu\right\}
\end{aligned}
\tag{8}
$$

We now use the fact that our function θ is related to the integrals appearing in the expressions of Shiomi and Hatsuda and Sarkar *et al.*.

$$\int_0^1 dx\,\ln[M^2 - k^2 x(1-x)] = -2 + 2\ln(M) + 2\theta$$

$$\int_0^1 dx\,x(1-x)\ln[M^2 - k^2 x(1-x)] = -\frac{5}{8} - \frac{2}{3}\frac{M^2}{k^2} + \frac{1}{3}\ln(M) - \frac{1}{3}\frac{(2M^2 + k^2)}{k^2}\theta$$

With these relations, it is straightforward to check that Eq. (8) coincides with the expression of Sarkar *et al.*

Scheme 5

The expression of Shiomi and Hatsuda can be recovered by the following recipe: First, one should subtract from the expressions of the functions $\mathcal{A}$, $\mathcal{B}$ from the preceding paragraph their values in the true vacuum $M = m$, and then, replace them in the expression[9] Eq. (7). In terms of our θ functions, one has

$$
\begin{aligned}
\Pi_{\rho\ vac(5)}^{\mu\nu} = \Pi_{\rho\ vac(S\&H)}^{\mu\nu} = {}& \left\{ \frac{g_\rho^2}{3\pi^2}\left[\ln M + \theta + \frac{2M^2}{k^2}(\theta - 1) - \frac{2}{k^2}(\theta_0 - 1) - \theta_0\right] \right. \\
& + \left(\frac{f_\rho}{2m}\right)^2 \frac{1}{6\pi^2}\left[6M^2\ln M + 8M^2\theta + k^2(\ln M + \theta) - 2(M^2 - 1) - (6M^2 + k^2 + 2)\theta_0\right] \\
& \left. + \frac{2M}{\pi^2}\left(\frac{f_\rho}{2m}\right)g_\rho\left[(\ln M + \theta - \theta_0)\right]\right\}\left\{k^2 g^{\mu\nu} - k^\mu k^\nu\right\}
\end{aligned}
\tag{9}
$$

Scheme 6

Another standard renormalization scheme is that used by Kurasawa and Suzuki [28] in the case of the σ and ω mesons. In this scheme, the conditions Eqs. (47,48) are applied at the physical mass $k^2 = \mu_\rho^2$ whereas conditions (49,50) are taken at $k^2 = 0$. The following expression is obtained

$$
\begin{aligned}
\Pi_{\rho\ vac(6)}^{\mu\nu} = {}& \left\{ \frac{g_\rho^2}{3\pi^2}\left[\ln M + \theta + \frac{2M^2}{k^2}(\theta - 1) - \frac{1}{\mu_\rho^2}\left((2 + \mu_\rho^2)\theta_\rho - 2\right)\right] \right. \\
& + \left(\frac{f_\rho}{2m}\right)^2 \frac{1}{6\pi^2}\left[6M^2\ln M + 8M^2\theta + k^2(\ln M + \theta) - (8 + \mu_\rho^2)\theta_\rho\right.
\end{aligned}
$$

---

[9]We note that this is not simply the same as subtracting the true vacuum from the total polarization, since the effective mass appears outside of $\widetilde{\mathcal{A}}$, $\widetilde{\mathcal{B}}$ in Eq. (7)

$$-(k^2 - \mu_\rho^2)\left((8 + \mu_\rho^2)\,\theta_{\rho k} + \theta_\rho\right) + 5 + 12M - 17M^2\Bigg]$$

$$+\frac{2}{\pi^2}\left(\frac{f_\rho}{2m}\right) g_\rho\left[M(\ln M + \theta) - \theta_\rho + 2(1 - M)\right]\Bigg\}\left\{k^2 g^{\mu\nu} - k^\mu k^\nu\right\} \tag{10}$$

Appendix C: Interaction potential in spatial coordinates

In this appendix, we give explicit expressions for the different meson contributions to the several pieces of the potential, as they appear in Eq. (56) : central, spin-orbit, spin-spin, tensor, and the nonlocal potential $V_{NL}(r)$.

A subscript will label these components, while the superscript indicates the meson which gives this contribution.

These expressions are valid when the rest frame of the background fluid coincides with the center of mass of the interacting particles.

Rho meson

$$V_c^{(\rho)}(r) = \frac{1}{2\pi^2 r}\int_0^\infty dq\, q\,\sin(qr)\,\mathcal{F}_\rho^2\left\{-g_\rho^2\, G_{\rho L}\left(1 - \frac{q^2}{4M}\right) + g_\rho\left(\frac{f_\rho}{2m}\right) G_{\rho L}\left(\frac{q^2}{M}\right)\right.$$
$$\left. + g_\rho^2\, G_{\rho T}\left(\frac{q^2}{4M^2}\right)\right\} \tag{1}$$

$$V_{SS}^{(\rho)}(r) = \left[g_\rho + 2M\left(\frac{f_\rho}{2m}\right)\right]^2 \frac{1}{12\pi^2 M^2\, r}\int_0^\infty dq\, q^3\,\sin(qr)\,\mathcal{F}_\rho^2\ G_{\rho T} \tag{2}$$

$$V_T^{(\rho)}(r) = \left[g_\rho + 2M\left(\frac{f_\rho}{2m}\right)\right]^2 \frac{1}{24\pi^2 M^2 r}\int_0^\infty dq\,\sin(qr)\,\mathcal{F}_\rho^2\left[\frac{3q}{r^2} - q^3\right] G_{\rho T}$$
$$- \left[g_\rho + 2M\left(\frac{f_\rho}{2m}\right)\right]^2 \frac{1}{8\pi^2 M^2 r^2}\int_0^\infty dq\, q^2\,\cos(qr)\,\mathcal{F}_\rho^2\, G_{\rho T} \tag{3}$$

$$V_{LS}^{(\rho)}(r) = \frac{1}{2\pi^2 M^2 r^3}\int_0^\infty dq\, q\,\sin(qr)\,\mathcal{F}_\rho^2\left\{g_\rho^2\left[\frac{G_{\rho L}}{2} + G_{\rho T}\right] + 2M\, g_\rho\left(\frac{f_\rho}{2m}\right)[G_{\rho L} + G_{\rho T}]\right\}$$
$$- \frac{1}{2\pi^2 M^2 r^2}\int_0^\infty dq\, q^2\,\cos(qr)\,\mathcal{F}_\rho^2\left\{g_\rho^2\left[\frac{G_{\rho L}}{2} + G_{\rho T}\right] + 2M\, g_\rho\left(\frac{f_\rho}{2m}\right)[G_{\rho L} + G_{\rho T}]\right\} \tag{4}$$

$$V_{NL}^{(\rho)}(r) = -\frac{g_\rho^2}{2\pi^2 M^2 r}\int_0^\infty dq\, q\,\sin(qr)\,\mathcal{F}_\rho^2\left[\frac{G_{\rho L}}{2} + G_{\rho T}\right] \tag{5}$$

with the following notations

$$G_{\rho L} = -G_\rho^{00}(q) = \frac{-1}{q^2 + \mu_\rho^2 - \Pi_\rho^{00}(0, q)} \qquad , \qquad G_{\rho T} = G_\rho^{11}(q) = \frac{-1}{q^2 + \mu_\rho^2 + \Pi_\rho^{11}(0, q)}$$

Sigma and omega mesons

The mixed σ-ω sector gives

$$V_c^{(\sigma\omega)}(r) = \frac{1}{2\pi^2 r}\int_0^\infty dq\, q\,\sin(qr)\left\{g_\sigma^2\mathcal{F}_\sigma^2\, G_\sigma\left(1 + \frac{q^2}{4M^2}\right) - g_\omega^2\mathcal{F}_\omega^2\, G_{\omega L}\left(1 - \frac{q^2}{4M^2}\right)\right.$$
$$\left. + g_\omega^2\,\mathcal{F}_\omega^2\, G_{\omega T}\left(\frac{q^2}{4M^2}\right) - 2g_\sigma g_\omega\,\mathcal{F}_\omega\mathcal{F}_\sigma\, G_{\sigma\omega}\right\} \tag{6}$$

$$V_{LS}^{(\sigma\omega)}(r) = \frac{1}{2\pi^2 M^2 r^3} \int_0^\infty dq\, q\, \sin(qr) \left\{ g_\sigma^2 \mathcal{F}_\sigma^2 \frac{G_\sigma}{2} + g_\omega^2 \mathcal{F}_\omega^2 \left[\frac{G_{\omega L}}{2} + G_{\omega T} \right] \right\}$$

$$- \frac{1}{2\pi^2 M^2 r^2} \int_0^\infty dq\, q^2\, \cos(qr) \left\{ g_\sigma^2 \mathcal{F}_\sigma^2 \frac{G_\sigma}{2} + g_\omega^2 \mathcal{F}_\omega^2 \left[\frac{G_{\omega L}}{2} + G_{\omega T} \right] \right\} \tag{7}$$

$$V_{NL}^{(\sigma\omega)}(r) = -\frac{1}{2\pi^2 M^2 r} \int_0^\infty dq\, q\, \sin(qr) \left\{ g_\sigma^2 \mathcal{F}_\sigma^2 \frac{G_\sigma}{2} + g_\omega^2 \mathcal{F}_\omega^2 \left[\frac{G_{\omega L}}{2} + G_{\omega T} \right] \right\} \tag{8}$$

$$V_{SS}^{(\sigma\omega)}(r) = \frac{g_\omega^2}{12\pi^2 M^2 r} \int_0^\infty dq\, q^3\, \sin(qr)\, \mathcal{F}_\omega^2\, G_{\omega T} \tag{9}$$

$$V_T^{(\sigma\omega)}(r) = \frac{g_\omega^2}{24\pi^2 M^2 r} \int_0^\infty dq\, \sin(qr)\, \mathcal{F}_\omega^2 \left[\frac{3q}{r^2} - q^3 \right] G_{\omega T}$$

$$- \frac{g_\omega^2}{8\pi^2 M^2 r^2} \int_0^\infty dq\, q^2\, \cos(qr)\, \mathcal{F}_\omega^2\, G_{\omega T} \tag{10}$$

In the above formulae, one has

$$G_\sigma = -\frac{q^2 + \mu_\omega^2 - \Pi_\omega^{00}(0,q)}{(q^2 + \mu_\sigma^2 + \Pi_\sigma(0,q))(q^2 + \mu_\omega^2 - \Pi_\omega^{00}(0,q)) + (\Pi_{\omega\sigma}^0(0,q))^2}$$

$$G_{\sigma\omega} = -\frac{\Pi_{\omega\sigma}^0(0,q)}{(q^2 + \mu_\sigma^2 + \Pi_\sigma(0,q))(q^2 + \mu_\omega^2 - \Pi_\omega^{00}(0,q)) + (\Pi_{\omega\sigma}^0(0,q))^2}$$

$$G_{\omega L} = -\frac{q^2 + \mu_\sigma^2 + \Pi_\sigma(0,q)}{(q^2 + \mu_\sigma^2 + \Pi_\sigma(0,q))(q^2 + \mu_\omega^2 - \Pi_\omega^{00}(0,q)) + (\Pi_{\omega\sigma}^0(0,q))^2}$$

$$G_{\omega T} = -\frac{1}{q^2 + \mu_\omega^2 + \Pi_\omega^{11}(0,q)}$$

<u>Pi meson</u>

Finally, the one-pion exchange only contributes to the spin-spin and tensor components :

$$V_{SS}^\pi(r) = \frac{g_\pi^2}{24\pi^2 M^2 r} \int_0^\infty dq\, q^3\, \sin(qr)\, \mathcal{F}_\pi^2\, G_\pi \tag{11}$$

$$V_T^\pi(r) = \frac{-g_\pi^2}{24\pi^2 M^2 r} \int_0^\infty dq \left[\frac{3q}{r^2} - q^3 \right] \sin(qr)\, \mathcal{F}_\pi^2\, G_\pi$$

$$+ \frac{g_\pi^2}{8\pi^2 M^2 r^2} \int_0^\infty dq\, q^2\, \cos(qr)\, \mathcal{F}_\pi^2\, G_\pi \tag{12}$$

where :

$$G_\pi(q) = \frac{-1}{q^2 + \mu_\pi^2 + \Pi_\pi(0,q)}$$

References

[1] R. Machleidt. 'The Meson Theory of Nuclear Forces and Nuclear Structure.' Adv. in Nucl. Phys. **Vol. 19**; J.W. Negele and E. Vogt Edts. (Plenum Press, New York, 1989.)

[2] B.D. Serot, J.D. Walecka, 'The Relativistic Nuclear Many-Body Problem', Adv. in Nucl. Phys., **Vol. 16**, J.W. Negele and E. Vogt Edts. (Plenum Press, New York, 1986).

[3] B.D. Serot and J.D. Walecka, *Int. J. Mod. Phys.* **E6** (1997) 515.

[4] R. Brockmann and R. Machleidt, *Phys. Rev.* **C42**, (1990), 1965.

[5] R. Brockmann and R. Machleidt : 'The Dirac-Brueckner Approach'. Prepared for 'Open Problems in Nuclear Matter' M. Baldo, ed. World Singapore. Preprint nucl-th/9612004.

[6] J. Friedel, *Phil. Mag.* **43** (1952) 153;
J. Friedel, *Nuovo Cim.* **7** (1958) Suppl. 2, 287.

[7] T.J. Rowland, *Phys. Rev.* **119** N3 (1960) 900.

[8] J. Kapusta and T. Toimela, *Phys. Rev.* **D37** (1988) 3731.

[9] W. Florkowski and B. Friman, *Nucl. Phys.* **A 611** (1996) 409.

[10] J. Diaz Alonso, A. Pérez and H. Sivak, *Nucl. Phys.* **A505** (1989) 695.

[11] E. Gallego, J. Diaz Alonso and A. Pérez, *Nucl. Phys.* **A578** (1994) 542.

[12] J. Diaz Alonso, E. Gallego and A. Pérez, *Phys. Rev. Lett.* V.73; N.19; (1994); 2536.

[13] J. Diaz Alonso and L. Mornas, *Nucl. Phys.* **A629** (1998) 679.

[14] N. Iwamoto, C.J. Pethick, *Phys. Rev.* **D25** (1982) 313.

[15] S. Reddy, M. Prakash, J.M. Lattimer and J.A. Pons, *Phys. Rev.* **C59** (1999) 2888.

[16] K. Wehrberger, *Phys. Rep.* **225** (1993) 273.

[17] A. D. Jackson and T. Wettig, *Phys. Rep.* **273** (1994) 325.

[18] J. Dukelsky and P. Schuck, *Nucl. Phys.* **A512** (1990) 466.

[19] Th. Bornath, D. Kremp and M. Schlanges, eprint physics/9903039

[20] J.M. Häuser, W. Cassing and A. Peter, *Nucl. Phys.* **A585** (1995) 727.
J.M. Häuser, W. Cassing, A. Peter and M.H. Thoma, *Z.Phys.* **A353** (1996) 301.

[21] J.C. Caillon and J. Labarsouque, *Nucl. Phys.* **A572** 649.

[22] G. Chanfray, R. Rapp and J. Wambach, *Phys. Rev. Lett.* **76** (1996) 368.

[23] J. Diaz Alonso and A. Pérez, *Nucl. Phys.* **A526** (1991) 623.

[24] J. Diaz Alonso, *Ann. Phys.* **160, N1** (1985), 1.

[25] S.A. Chin, *Ann. Phys. (N.Y.)* **108** (1977), 301.

[26] J. Diaz Alonso and R. Hakim, *Phys. Lett.* **A 66**, (1978), 476.

[27] H. Shiomi and T. Hatsuda, *Phys. Lett.* **B334** (1994) 281.

[28] H. Kurasawa, T. Suzuki, *Nucl. Phys.* **A490** (1988) 571.

[29] S. Sarkar, J. Alam, P. Roy, A. Dutt-Mazumder, B. Dutta-Roy and B. Sinha, *Nucl. Phys.* **A634** (1998) 206.

[30] J. Diaz-Alonso, L. Mornas and M.A. Pérez-García, in preparation

[31] J. Diaz Alonso and L. Mornas, *Phys. Lett* **B437** (1998) 12-18.

[32] K. Lim and C.J. Horowitz, *Nucl. Phys.* **A501** (1989) 729.

[33] J. Diaz-Alonso, private communication.

[34] G. E. Brown and M. Rho, *Phys. Rev. Lett.* **66** (1991) 2720.

[35] T. Hatsuda and Su H. Lee, *Phys. Rev.* **C46** (1992) R34.

[36] Xuemin Jin and D.B. Leinweber, *Phys. Rev.* **C52** (1995) 3344.

[37] D.K. Griegel and T. D. Cohen, *Phys. Lett.* **B333** (1994) 27.

[38] S. Leupold, W. Peters and U. Mosel, *Nucl.* Phys **A628** (1008)

[39] F. Klingl, N. Kaiser and W. Weise, *Nucl. Phys.* **A624** (1997) 527.

[40] A. Nyffeler, LANL eprint hep-ph/0010329

[41] D. Cabrera, E. Oset and M.J. Vicente Vacas, LANL preprint nucl-th/0011037

[42] R. Rapp and J. Wambach, LANL preprint hep-ph/9909229

[43] K. Saito, K. Tsushima and A.W. Thomas, *Phys. Rev.* **C55** (1997) 2637;
K. Saito, K. Tsushima and A.W. Thomas, *Phys. Rev.* **C56** (1997) 566.

[44] M. Herrmann, B.L. Friman and W. Nörenberg, *Nucl. Phys.* **A560** (1993) 411.

[45] F. Klingl, N. Kaiser and W. Weise, *Z. Phys.* **A356** (1996) 193.

[46] R.D. Pisarski, *Nucl. Phys.* **A590** (1995) 553c;
R.D. Pisarski, *Phys. Rev.* **D52** (1995) 3773.

[47] C. Song, *Phys. Rev.* **D48** (1993) 1375

[48] M. Masera *el al*, HELIOS collaboration, *Nucl. Phys.* **A590** (1992) 93c.

[49] G. Agakichiev *et al.*, CERES collaboration, *Phys. Rev. Lett.* **75** (1995) 1272;
G. Agakichiev *et al.*, CERES collaboration, *Phys. Lett.* **B422** (1998) 405

[50] G.Q. Li and C.M. Ko, *Nucl. Phys.* **A582** (1994) 731.

[51] C. M. Ko, G. Q. Li, G. E. Brown and H. Sorge, *Nucl. Phys.* **A610** (1996) 342c.

[52] W. Cassing, W. Ehehalt and C.M. Ko, *Phys. Lett.* **B363** (1995) 35.

[53] R. Rapp, G. Chanfray and J. Wambach, *Nucl. Phys.* **A617** (1997) 472.

[54] B. Friman and H.J. Pirner, *Nucl. Phys.* **A617** (1997) 496.

[55] J. B. McClelland *et al.*, *Phys. Rev. Lett.* **69** (1992) 582.

[56] G. E. Brown and J. Wambach, *Nucl. Phys.* **A568** (1994) 895.

[57] W. Unkelbach, C. Glashausser, A. Green and J. Wambach, *Nucl. Phys.* **A569** (1994) 353c.

[58] K. Yoshida and H. Toki, *Nucl. Phys.* **A648** (1999) 75.

[59] J. Diaz Alonso, A. Pérez and H. Sivak, hep-ph/9803344.

[60] C. E. Price, J. R. Shepard and J. A. McNeil, *Phys. Rev.* **C 41**, (1990) 1234;
C. E. Price, J. R. Shepard and J. A. McNeil, *Phys.Rev.* **C 42**, (1990) 247.

[61] M. Urban, M. Buballa, R. Rapp, J. Wambach, Nucl. Phys. **A673** (1999) 357.

[62] W. Cassing, E.L. Bratkovskaya, Phys. Rep. **308** (1999) 65.

[63] M. Asakawa, C.M. Ko, *Phys. Rev.* **C48** (1993) R526;
M. Asakawa, C.M. Ko, P. Levai, X.J. Qiu, *Phys. Rev.* **C46** (1992) R1159.

[64] M. Baldo, I. Bombaci, G. Giansiracusa, U. Lombardo, C. Mahaux and R. Sartor, *Phys. Rev.* **C41** (1990) 1748.

[65] F. de Jong and R. Malfliet, *Phys. Rev.* **C44** (1991) 998.

[66] J. Diaz Alonso and R. Hakim, *Phys. Rev.* **D 29** (1984), 2690.

Figure 1: Schematic representation of the Schwinger-Dyson equation for the meson propagators.
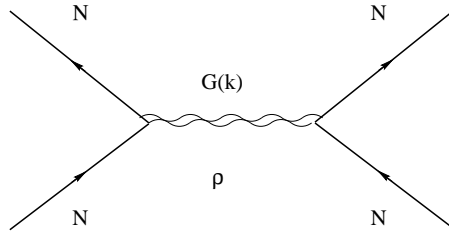

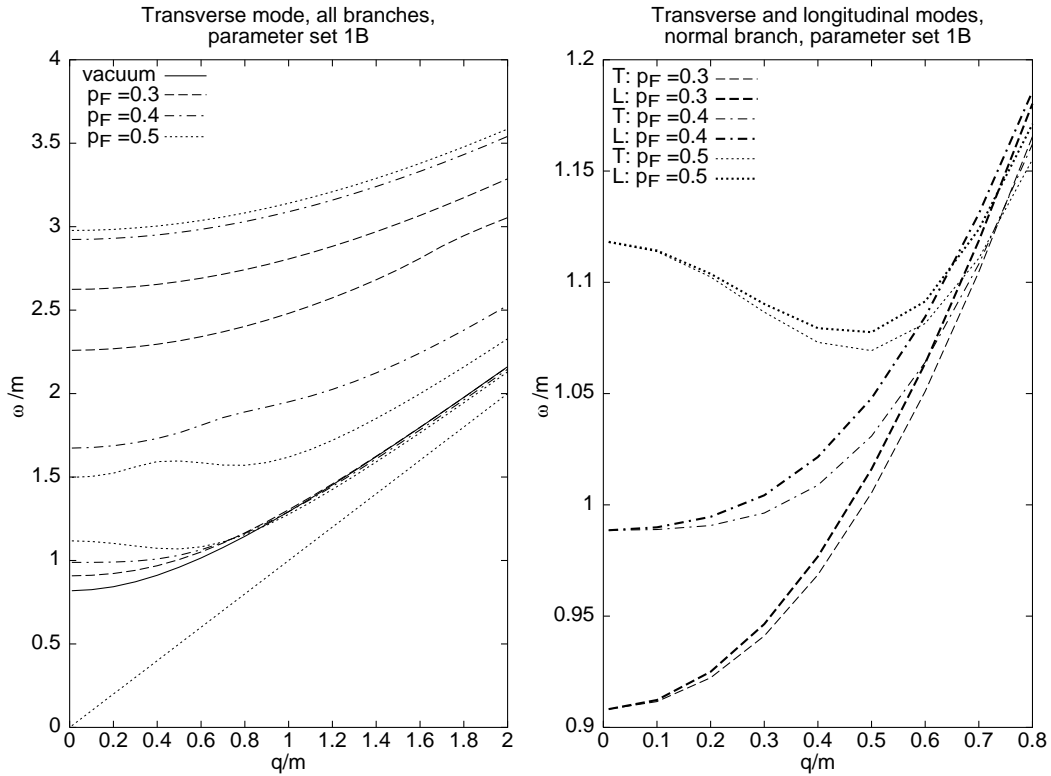Figure 2: Diagram for one-rho meson exchange. The double line represents the in-medium rho meson propagator.

Figure 3: Rho-meson dispersion relations for parameter set 1B. The solid line correspond to vacuum density, and the dashed, dot-dashed and dotted lines to finite density with a value of Fermi momentum p_F/m=0.3, 0.4, 0.5 respectively. The left panel shows transverse modes. There are normal and heavy meson branches. The right panel compares longitudinal (thick lines) to transverse modes (thin lines) for the normal branch. We use the same conventions as in the left panel to represent various densities. Magnitudes are given in units of the free nucleon mass m.
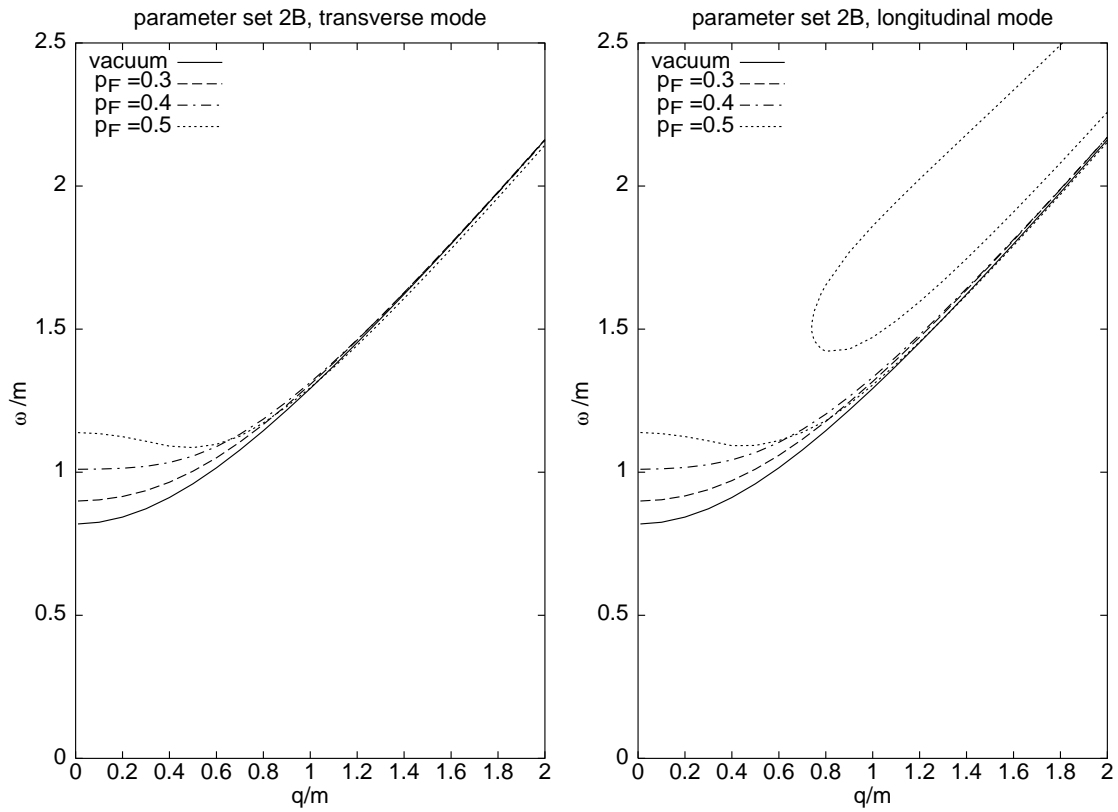
Figure 4: Rho-meson dispersion relations for parameter set 2B. The left panel shows the transverse branch at various density with the same conventions as in Fig. 3. Only the normal branch remains in this case. The longitudinal branches are represented in the right panel. Besides the normal branch, we have a remnant of the heavy meson modes at high density.
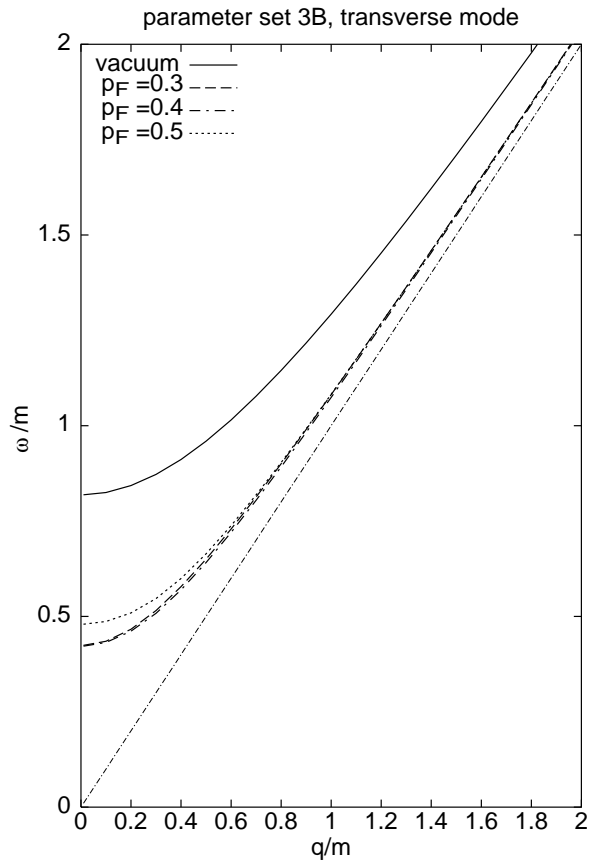
Figure 5: Rho-meson dispersion relation for parameter set 3B. Only the transverse branch is shown. The longitudinal branch almost coincides with the transverse one so that it could not be distinguished by eye from the former. Only normal branches are present in this case
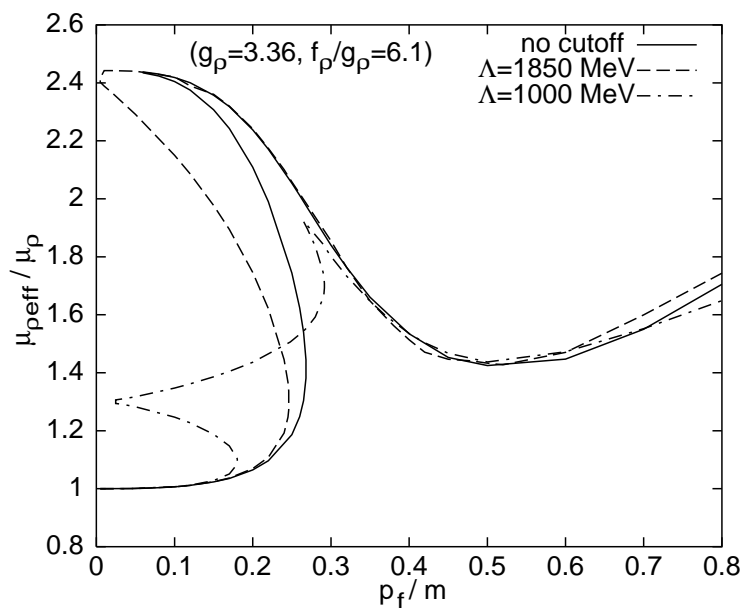
Figure 6: In-medium ρ-meson mass as a function of the nuclear Fermi momentum, when the vacuum term is discarded. For small densities, it would appear that the effective rho mass increases; however neglecting of vacuum fluctuations is at the origin of an unpleasant cusp, which cannot be removed even by very low values of the cutoff parameter in the form factor
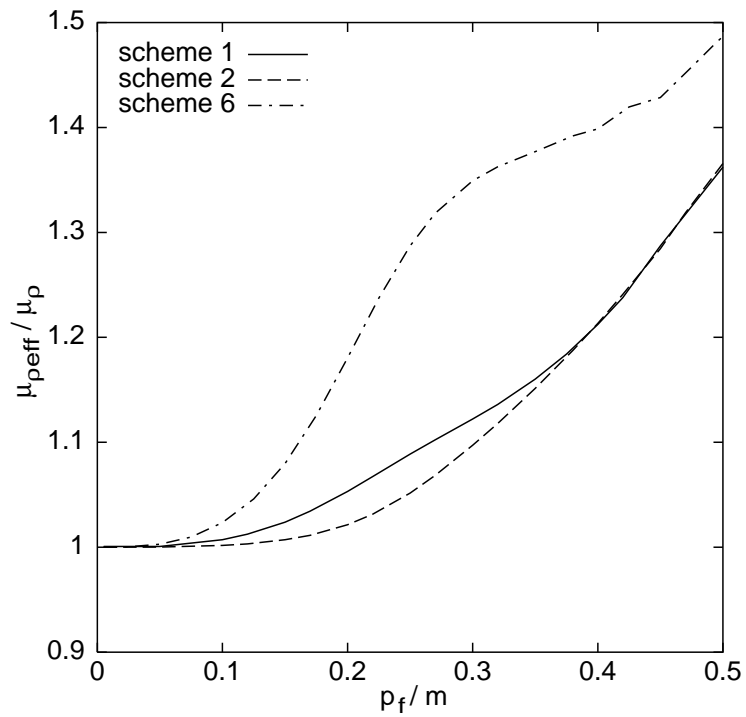
Figure 7: In-medium ρ-meson mass as a function of the nuclear Fermi momentum. Vacuum polarization is included according to the first class of renormalization schemes 1, 2 and 6 (= "Kurasawa-Suzuki").
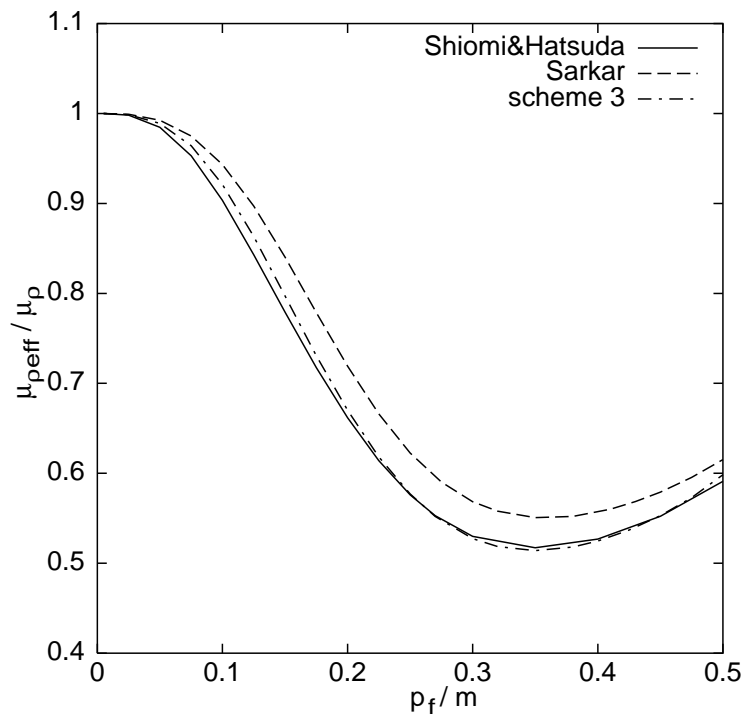
Figure 8: In-medium ρ-meson mass as a function of the nuclear Fermi momentum. Vacuum polarization is included according to the second class of renormalization schemes 3, 4 (= " Sarkar") and 5 (= "Shiomi-Hatsuda").
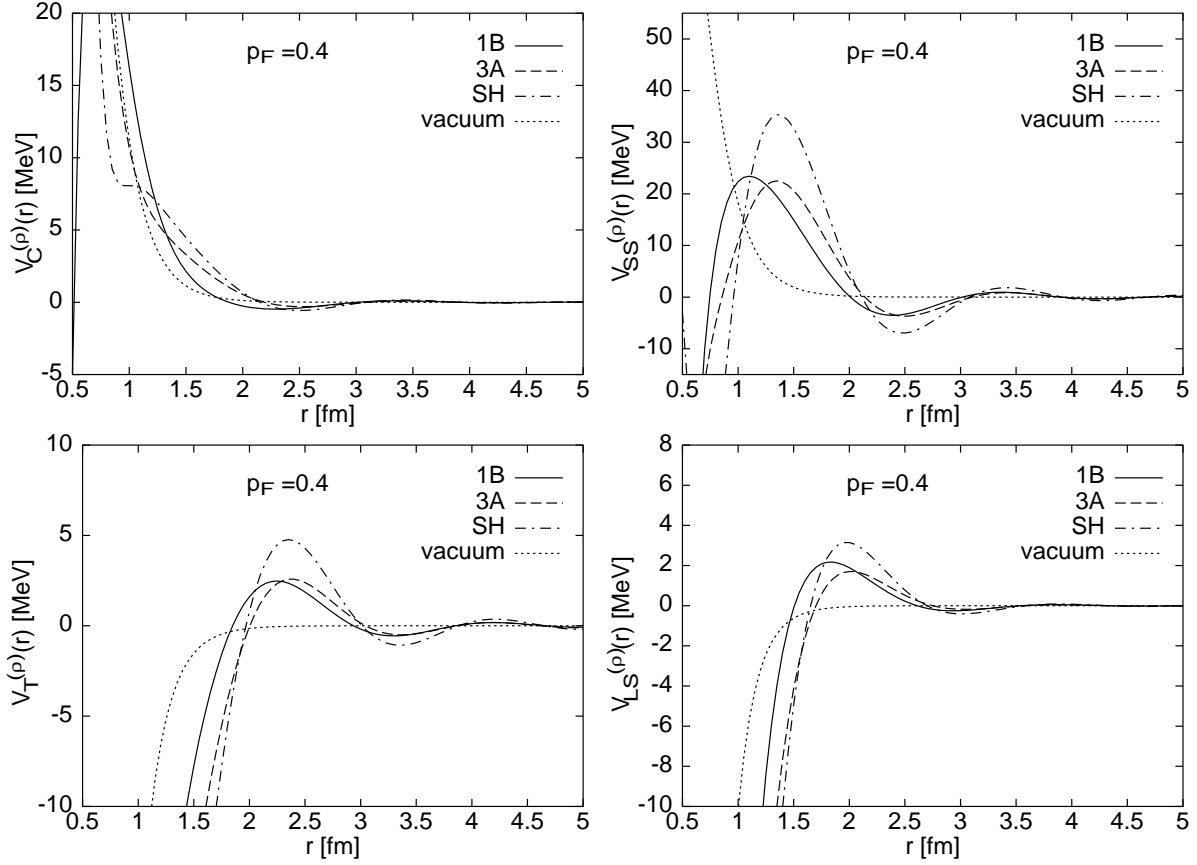
Figure 9: One-rho exchange component of the potential at 2.4 times saturation density (p_F=0.4) for various renormalization schemes: scheme 1 with parameter set 1B (solid line), scheme 3 with parameter set 3A (dashed line) and scheme 5 (= "Shiomi-Hatsuda") with the parameter set of Machleidt Bonn-B potential (dot-dashed line). The potential in vacuum is also shown for reference (dotted line). The left upper panel shows the central component, the right upper panel displays the spin-spin component, the left lower panel corresponds to the tensor part. Finally the spin-orbit component is represented in the right lower panel.
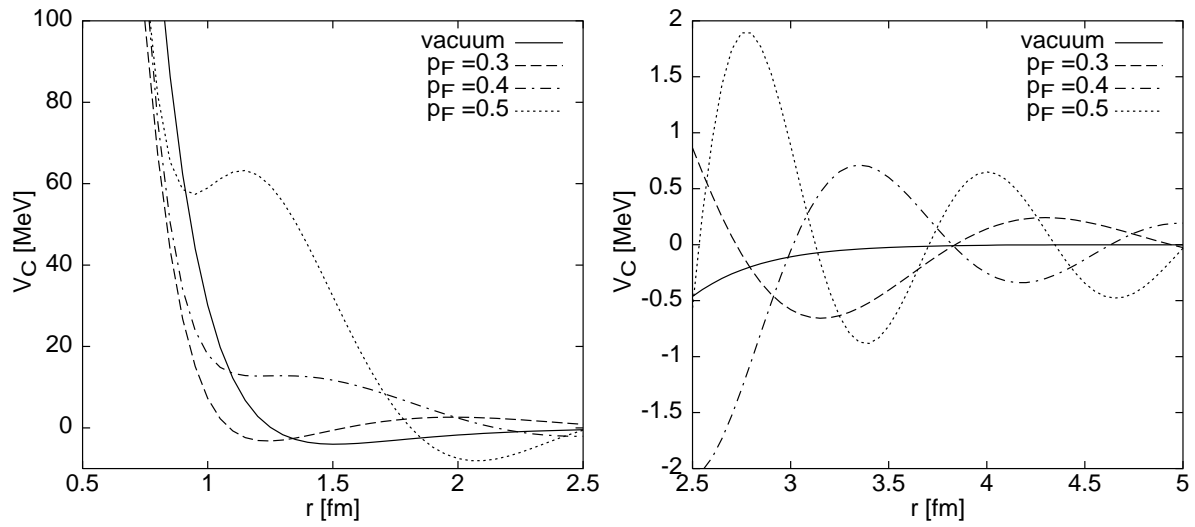
Figure 10: Central component of the potential including all $(\sigma, \omega, \rho, \pi)$ mesons in the medium, using parameter set 1B with renormalization scheme 1. We use the same conventions as in the left panel to represent various densities. The left panel represents the short range part of the potential. The right panel illustrates the oscillatory behavior in the long range part.
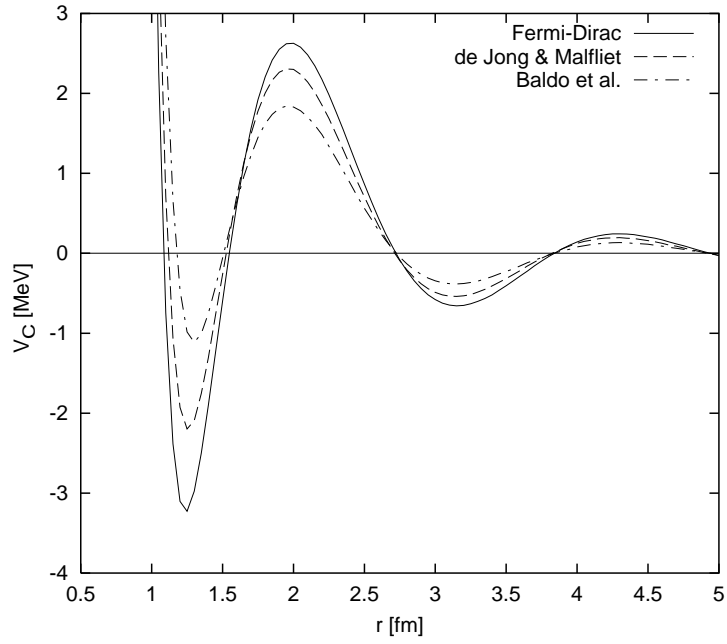
Figure 11: Influence of the rounding off of the momentum distribution function on the amplitude of Friedel oscillations. We show the central component of the potential including all mesons at saturation density and vanishing temperature, using parameter set 1B with renormalization scheme 1. The solid line was obtained for a Fermi-Dirac distribution (as in previous figures). The dashed line uses the parametrization of the result of a (relativistic) Dirac-Brueckner-Hartree Fock calculation by de Jong and Malfliet [58]. The dash-dotted line uses the parametrization of the result of a (nonrelativistic) Brueckner-Hartree Fock calculation by Baldo *et al.* [57].
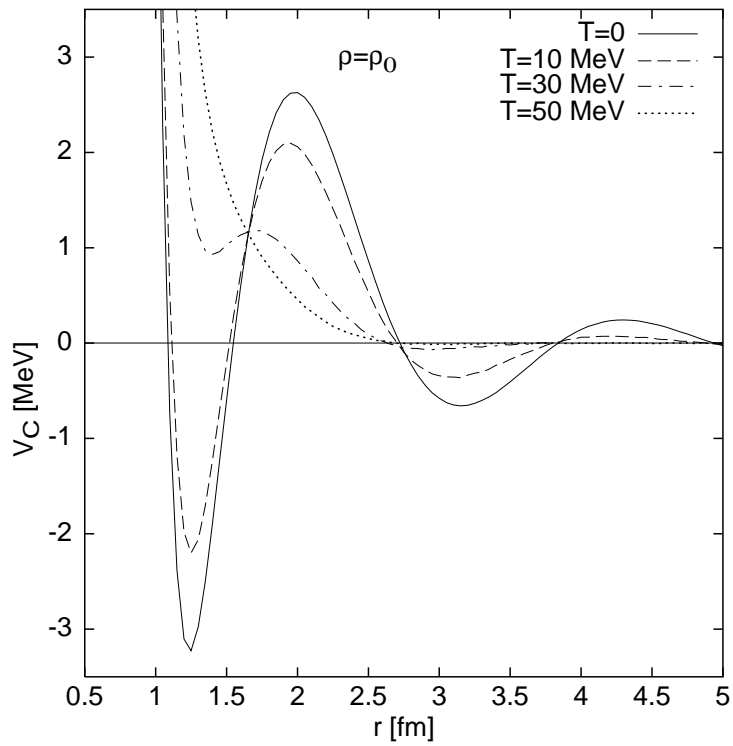
Figure 12: Influence of temperature on the amplitude of oscillations. We show the central component of the potential including all mesons at saturation density, using parameter set 1B. The solid, dashed, dot-dashed and dotted lines correspond to temperatures T=0, 10, 30, 50 MeV respectively.